Nanoscale

PAPER

View Article Online
View Journal | View Issue

Cite this: *Nanoscale*, 2015, **7**, 17710

The functional dissection of the plasma corona of SiO_2-NPs spots histidine rich glycoprotein as a major player able to hamper nanoparticle capture by macrophages†

Chiara Fedeli,[a,b] Daniela Segat,‡[c] Regina Tavano,[a,b] Luigi Bubacco,[c] Giorgia De Franceschi,[a] Patrizia Polverino de Laureto,[a] Elisa Lubian,[d] Francesco Selvestrel,[d] Fabrizio Mancin*[d] and Emanuele Papini*[a,b]

A coat of strongly-bound host proteins, or *hard corona*, may influence the biological and pharmacological features of nanotheranostics by altering their cell-interaction selectivity and macrophage clearance. With the goal of identifying specific corona-effectors, we investigated how the capture of amorphous silica nanoparticles (SiO_2-NPs; Ø = 26 nm; zeta potential = –18.3 mV) by human lymphocytes, monocytes and macrophages is modulated by the prominent proteins of their plasma corona. LC MS/MS analysis, western blotting and quantitative SDS-PAGE densitometry show that Histidine Rich Glycoprotein (HRG) is the most abundant component of the SiO_2-NP hard corona in excess plasma from humans (HP) and mice (MP), together with minor amounts of the homologous Kininogen-1 (Kin-1), while it is remarkably absent in their Foetal Calf Serum (FCS)-derived corona. HRG binds with high affinity to SiO_2-NPs (HRG K_d ~2 nM) and competes with other plasma proteins for the NP surface, so forming a stable and quite homogeneous corona inhibiting nanoparticles binding to the macrophage membrane and their subsequent uptake. Conversely, in the case of lymphocytes and monocytes not only HRG but also several common plasma proteins can interchange in this inhibitory activity. The depletion of HRG and Kin-1 from HP or their plasma exhaustion by increasing NP concentration (>40 μg ml^{-1} in 10% HP) lead to a heterogeneous hard corona, mostly formed by fibrinogen (Fibr), HDLs, LDLs, IgGs, Kallikrein and several minor components, allowing nanoparticle binding to macrophages. Consistently, the FCS-derived SiO_2-NP hard corona, mainly formed by hemoglobin, α2 macroglobulin and HDLs but lacking HRG, permits nanoparticle uptake by macrophages. Moreover, purified HRG competes with FCS proteins for the NP surface, inhibiting their recruitment in the corona and blocking NP macrophage capture. HRG, the main component of the plasma-derived SiO_2-NPs' *hard corona*, has antiopsonin characteristics and uniquely confers to these particles the ability to evade macrophage capture.

Received 5th August 2015,
Accepted 15th September 2015

DOI: 10.1039/c5nr05290d

www.rsc.org/nanoscale

Introduction

The success of the huge effort devoted to design effective nanoparticles (NPs) for therapy and diagnosis strongly needs parallel investigations on the interactions of such systems with biological media. Indeed, only by understanding the interplay between nanoparticles and biological entities it will be possible to rationally plan the desired action mechanism of nanotheranostics. It is now well established that the surface of the nanoparticle is a crucial variable determining such interactions and consequently the nanoparticle's biological effects. On the other hand, it is also quite clear that the first event occurring to the nanoparticle, once entered in a biological environment, is the formation of a surface adsorbed layer of proteins, named the *protein corona*.[1–15] The protein corona

[a]*Centro di Ricerca Interdipartimentale per le Biotecnologie Innovative, Università di Padova, via U. Bassi 58/B, I-35131 Padova, Italy. E-mail: emanuele.papini@unipd.it*
[b]*Dipartimento di Scienze Biomediche, Università di Padova, via U. Bassi 58/B, I-35131 Padova, Italy*
[c]*Dipartimento di Biologia, Università di Padova, via U. Bassi 58/B, I-35131 Padova, Italy*
[d]*Dipartimento di Scienze Chimiche, Università di Padova, via Marzolo 1, I -35131 Padova, Italy. E-mail: fabrizio.mancin@unipd.it*

†Electronic supplementary information (ESI) available: Additional uptake and corona characterization experiments, protein purification, DLS experiments, protein affinity and geometrical calculations, and protein tables. See DOI: 10.1039/c5nr05290d

‡Current address: Institute for Rare Diseases 'Mauro Baschirotto', *via* B. Bizio 1, 36023 Costozza di Longare (Vicenza), Italy.

formation *in vivo* is likely a major actor at the host/nanoparticle interface, deeply influencing the bioactivity and the bioavailability of nanosystems.[16] Available evidence suggests that the protein corona composition varies depending on several factors including the nanoparticle material, surface functionalization, size, shape and the biological environment. Although relatively small subsets of the many proteins available in biological fluids are normally found to bind nanoparticles, still the reported corona compositions involve from tens to a few hundreds of polypeptides. Simple geometric considerations make it however difficult to rationalize, especially for small nanoparticles (<30 nm diameter), the physical coexistence in the same corona of hundreds of different protein types, in particular when one considers that some of them have a size comparable to or even larger than the NP itself. In fact, semi-quantitative estimations by label-free methods after shotgun LC MS/MS analysis show that, beside few main corona components, expected to cover the major part of the NP surface, the majority of the other polypeptides found associated with the NPs are indeed present in substoichiometric ratios (<1 polypeptide per nanoparticle).[12–14] This observation somehow resolves the paradox of accommodating too many components in the same corona, but introduces an additional level of heterogeneity of the corona-coated NPs, because it implies the presence of several subsets of nanoparticles each characterized by its own corona, with fewer polypeptides but with specific composition differences. Additional complexity is provided by the fact that the first shell of strongly bound proteins (hard corona) can reversibly interact with other proteins forming the so called *soft corona* and enlarging the number of proteins coating the nanoparticle.[17]

The above considerations may suggest that the goal of fully understanding the nanoparticle corona functional complexity, with the aim to predict the biocompatibility and pharmacological properties of a candidate nanosystem, may be a too demanding task. On the other hand, recent statistical and correlative studies with gold NPs indicate that small subsets of the corona polypeptides (6–10 out of the ~400 found) may be the major functional actors influencing the nanoparticle biological characteristics, and the detection of their presence in the corona has been proposed as a useful tool to predict nanoparticles' efficacy to enter cells.[5] Therefore, the functional discrimination of the corona components that *play the lead roles* from *background actors*, and the definition of the nanoparticle surface features controlling their selection, may become mandatory information for the design of efficient theranostic nanosystems. To achieve this goal, the individuation of simplified models for corona investigations and the calibration of suitable experimental conditions and test candidates capable of providing really predictive data are of paramount importance.[18]

In this paper we focus our attention on silica nanoparticles (SiO_2-NPs), which have attracted great attention as potential nanomedicine candidates[19] and on monocytes and macrophages, phagocytic cells of the reticular endothelial system (RES)/mononuclear phagocyte system (MPS). Indeed, these cells are especially exposed to nanoparticles after blood injection, due to their particulate capturing specialization, and represent a good starting point to understand the interaction of nanoparticles with biological entities and how the protein corona can affect the nanoparticle properties. It may be expected that nanoparticles efficiently internalized by such cells will be rapidly removed by circulation *in vivo* and accumulated in the main filtering organs, the liver and spleen. On the contrary, nanoparticles capable of escaping phagocytic capture will circulate longer and may eventually reach different tissues. The central role of RES/MPS clearance in determining the efficacy of nanotheranostics has recently been highlighted in mice models and humans.[20]

One of the acknowledged effects of the protein corona is the reduction of nanoparticle uptake by many cell types.[21,22] We have previously reported that such a protection activity is present in lymphocytes, used as a representative of cells without phagocytic activity, and in monocytes, when incubated with 30 nm-diameter SiO_2-NPs in the presence of Foetal Calf Serum (FCS), but is remarkably not present in macrophages.[23,24] With these cells, SiO_2-NP capture in FCS is very high and comparable to that observed in protein free media. Such a behaviour has been reported also for other nanomaterials under similar conditions.[25] However, extrapolation to the human context is dubious[26] especially because proteomic analysis clearly indicates that the nanoparticle protein hard-corona formed in FCS is distinctively different from that formed in human plasma (HP).[21,27] Moreover coagulation and complement components, immunoglobulins (IgG) and lipoproteins are defective in FCS compared to HP.[28]

In this view, we explored and compared the composition of the coronas formed on SiO_2-NPs upon incubation with different protein sources, *i.e.* the commonly used Foetal Calf Serum (FCS), mouse plasma (MP) and human plasma (HP). In doing this, we paid close attention to the effect of the nanoparticle dose on the corona composition. Eventually, we ascertained the role of the single major proteins composing the corona formed in HP in determining the interaction of the nanoparticles with phagocytic or non-phagocytic cells. Interesting and stimulating results emerged from this investigation: (i) the hard-corona formed in HP strongly changes the cell binding selectivity of SiO_2-NPs compared to the FCS-derived hard-corona; (ii) a single protein, namely Histidine Rich Glycoprotein (HRG), emerges as the main component of the HP/MP-derived SiO_2-NPs' hard-corona, but not of the FCS-derived one, and is responsible for the different behaviour of the nanoparticles in the two biofluids; (iii) HRG uniquely confers to SiO_2-NPs the ability to reduce macrophage capture *in vitro*, a specific stealthing property missing in other major human plasma proteins.

Results

Differential effect of FCS and HP on SiO_2-NP macrophage binding

To gain more insight into the role played by the plasma protein corona in cell interactions, we prepared fluorescein-

labelled 26 nm-diameter silica nanoparticles, produced by the Stöber–Van Blaaderen protocol,[29–31] and analysed their uptake by HepG2, a cell line from human hepatocarcinoma, primary human lymphocytes, monocytes and macrophages in the absence of proteins and in the presence of FCS and HP (both 10% v/v). Low nanoparticle doses (<40 μg ml^{-1}) were used both to avoid potential confounding factors arising from cytotoxic and proinflammatory effects and to better simulate the high dilution conditions presumably experienced by nanoparticles after injection in the bloodstream. The results obtained are very interesting (Fig. 1). In agreement with previous observations, cell capture of SiO_2-NPs, after 3 hours in protein-free media, is strongly inhibited by FCS in HepG2, lymphocytes and monocytes (>80% > 99% > 95% inhibition respectively) while not affected in macrophages.[23,24] The behaviour observed in human plasma (HP) is substantially different. Indeed, incubation in this medium results in an increased inhibition of SiO_2-NP uptake by HepG2 cells, lymphocytes and monocytes and, different from FCS, also by macrophages (~90–95% inhibition). This protective effect of HP is particularly efficient at low particle doses (<20 μg ml^{-1}) and is still observed after prolonged incubation times under the same conditions up to 20 h (Fig. S1†).

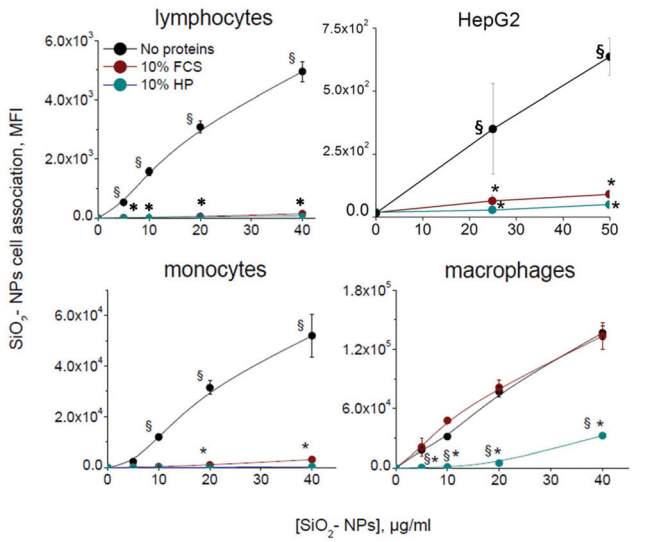

Fig. 1 Comparison of the effects of FCS and HP on the binding of SiO_2-NPs to lymphocytes, HepG2, monocytes and macrophages. The indicated cells were incubated in RPMI 1640 medium without proteins (no proteins), plus 10% (v/v) FCS or 10% (v/v) HP, as indicated, for 3 h at 37 °C with SiO_2-NPs at the indicated concentrations, and analysed by flow cytometry. Data, expressed as the mean fluorescence intensity, were acquired keeping the same instrument settings to ensure comparison. Note that *Y* axis scales are different in the four cells. Values are the means from experiments run in duplicate ± SE (N = 4). * significance (p < 0.05) with respect to no protein; § significance (p < 0.05) with respect to FCS.

Characterization of the SiO_2-NP corona composition in FCS and in human and mouse plasma

A reasonable hypothesis to explain the observed difference between HP and FCS in affecting SiO_2-NPs' macrophage uptake is that one or more proteins selectively present in the HP-derived NP corona, while not in the FCS-derived one, can hamper the special ability of macrophages to engage NPs. Therefore, we analysed the protein corona formed on nanoparticles incubated for 15 minutes at 37 °C in the two media. After NP recovery and extensive washing by ultracentrifugation, the associated proteins were subjected to gradient gel electrophoresis under non-reducing conditions, evidenced by the very sensitive silver staining and eventually analysed by densitometry (Fig. 2).

Both the apparent molecular weight and the intensity of the major bands, in agreement with other studies,[21,27] confirm that the pattern of the main proteins strongly associated with NPs varies considerably depending on the protein medium.

Moreover, the protein pattern also varies with the nanoparticle concentration, particularly in the case of HP. In this medium a peculiar observation is that, at NP concentrations below 40 μg ml^{-1}, a single protein band with an apparent MW of 60 kDa (p60) predominates in the pattern, while above this

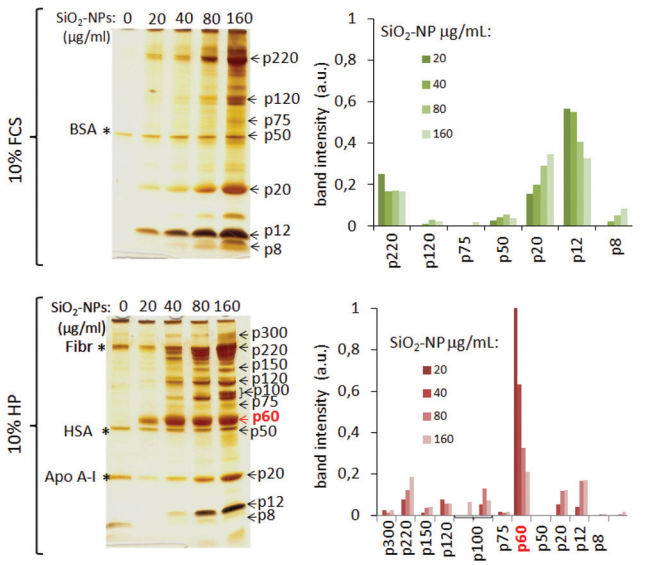

Fig. 2 SDS-PAGE analysis of the pattern of FCS and HP proteins adsorbed on SiO_2-NPs. SiO_2-NPs were incubated at the indicated concentrations for 15 minutes at 37 °C in RPMI 1640 plus 10% FCS or 10% HP, as specified, isolated and subjected to 4–20% gradient SDS-PAGE (left). Equal sample volumes and so increasing NP amounts per lane were loaded. After silver staining, a semi-quantitative estimation of the relative amount of the main protein bands found (arrows), labelled by their rough apparent molecular weight in kDa (pxx), were determined by densitometry and represented in histograms (right). The intensity of each band was normalized over the sum of the intensities of all the bands within the same lane. * indicates the major background proteins present in the samples treated without NPs (mock samples) and recovered from FCS (BSA) and HP (Fibr, HSA, Apo A-I). Gels are from representative experiments out of four.

dose (NPs 80–160 μg ml^{-1}) several other protein bands, either with higher or with lower molecular weights become also evident. The main bands observed (7 for FCS and 12 for HP) were then analysed by LC MS/MS to obtain a semi-quantitative evaluation of their polypeptide composition and relative proportion, using well-established bioinformatics label-free parameters.[32] In 10% FCS (Fig. 3A and Table S1† for detailed MS analysis), the major electrophoretic bands correspond to haemoglobin (p12), α2-macroglobulin (p220) and HDL-associated Apo A-I (p20). Other constituents are HDL-associated Apo A-II (p8), albumin (p50), complement Factor H (Fh) (p120) and plasminogen (PLG) (p75).

A remarkably different pattern was found with 20 μg ml^{-1} SiO_2-NPs in 10% HP (Fig. 3B and Table S2† for detailed MS analysis). Here, based on emPAI label free evaluation, using a cut of >1 significant peptides identified,[33] the most stained band (p60) was found to be essentially made by HRG (70% HRG, 11% Kin-1) while the second less intense one (p100) was mostly formed by Kin-1 (76% Kin-1 and 13% HRG). At the NP concentration of 160 μg ml^{-1} the p60 band was still present and was again formed by HRG (HRG 86%, vitronectin 14%) but within the context of a more complex set of bands. Focusing on major components, it can be noted that the p300 band is formed by Fibr (93%) and by the LDL marker Apo B-100 (7%) similarly to p220 (Fibr 83% Apo B-100 17%); p150 is a mixture of IgG (66%), SERPING1 (16%) and KLK (11%); p120 is more heterogeneous (32% Apo B-100 fragment, 28% Kallikrein, 16% HRG and 16% plasma serine protease C1 inhibitor); the two close bands p100′/p100″ both corresponded to Kin-1 (Kin-1 91%, HRG 8%); the faint p75 band was heterogeneous (25% Apo E, 17% Kin-1, 13% PLG). Band p50 was made principally by HSA (61%) and by a mixture of other minor proteins Apo A-I being the most relevant (17%). However, it is important to note that this band seems to be present with a similar intensity also in the mock NP free sample, indicating that it may be a remnant from plasma. Band p20 is ~100% formed by the HDL marker Apo A-I, while p12 is mostly Apo A-II (87%, Apo A-I 13%) and p10 is made by SAA-4 67% plus a fragment of the LDL maker Apo E (26%).

After correction of emPAI for sample loading, which varied for different bands to ensure sufficient counts for the faintest bands, and correction for quaternary structures, when necessary, we could obtain an estimation of the relative molar content of the found proteins associated with the NPs (Fig. S2A and B†). The results are in good agreement with densitometry estimation and indicate that at low NP doses HRG and Kin-1 are the major proteins accounting for more than 90% of the total proteins. Again in agreement with densitometry, HRG and Kin-1 are still present at 160 μg ml^{-1}, about 10% of total proteins each, but several other proteins are now detected. Among these the most prevalent are Ig (8%), Fibr (14%), LDL (16%) (using Apo B-100 and Apo E as bona fide markers) and HDL (18%) (using Apo A-I and Apo A-II as bona fide markers). The amounts of the major polypeptides forming the HP-derived protein coronas did not change grossly on increasing the incubation time of the nanoparticles up to 6 hours (Fig. S3†), indicating that the composition observed represents the kinetically stable state (hard corona) under the experimental conditions.

Since in other studies the protein corona forming around SiO_2 and other NPs was analysed after incubation at 0–4 °C and in the presence of higher HP concentrations,[11,34] we tested the prevalence of HRG also under these conditions

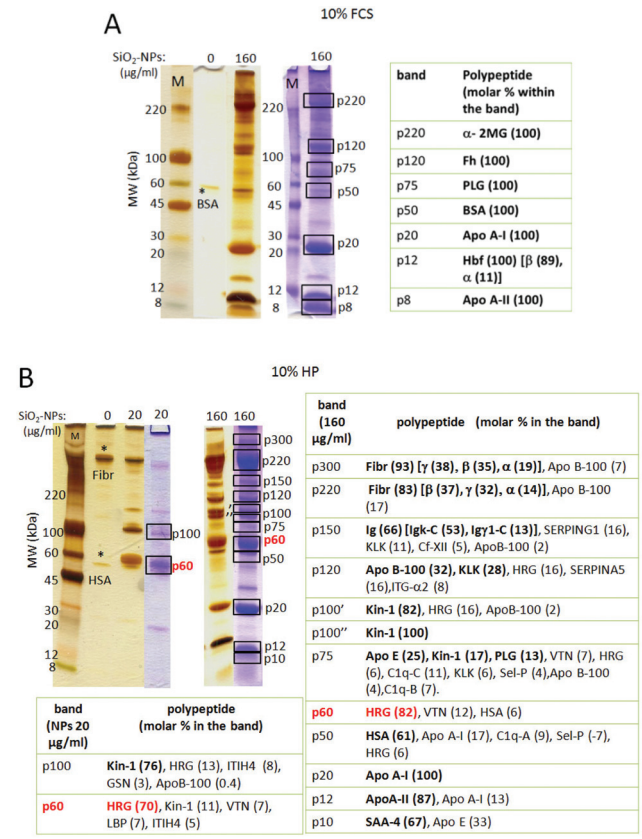

band	Polypeptide (molar % within the band)
p220	α- 2MG (100)
p120	Fh (100)
p75	PLG (100)
p50	BSA (100)
p20	Apo A-I (100)
p12	Hbf (100) [β (89), α (11)]
p8	Apo A-II (100)

band (NPs 20 μg/ml)	polypeptide (molar % in the band)
p100	Kin-1 (76), HRG (13), ITIH4 (8), GSN (3), ApoB-100 (0.4)
p60	HRG (70), Kin-1 (11), VTN (7), LBP (7), ITIH4 (5)

band (160 μg/ml)	polypeptide (molar % in the band)
p300	Fibr (93) [γ (38), β (35), α (19)], Apo B-100 (7)
p220	Fibr (83) [β (37), γ (32), α (14)], Apo B-100 (17)
p150	Ig (66) [Igk-C (53), Igγ1-C (13)], SERPING1 (16), KLK (11), Cf-XII (5), ApoB-100 (2)
p120	Apo B-100 (32), KLK (28), HRG (16), SERPINA5 (16),ITG-α2 (8)
p100′	Kin-1 (82), HRG (16), ApoB-100 (2)
p100″	Kin-1 (100)
p75	Apo E (25), Kin-1 (17), PLG (13), VTN (7), HRG (6), C1q-C (11), KLK (6), Sel-P (4),Apo B-100 (4),C1q-B (7).
p60	HRG (82), VTN (12), HSA (6)
p50	HSA (61), Apo A-I (17), C1q-A (9), Sel-P (-7), HRG (6)
p20	Apo A-I (100)
p12	ApoA-II (87), Apo A-I (13)
p10	SAA-4 (67), Apo E (33)

Fig. 3 Characterization of the pattern of FCS and HP polypeptides adsorbed on SiO_2-NPs by LC MS/MS. The SDS-PAGE bands, in yellow boxes, corresponding to the major corona proteins formed on SiO_2-NPs after incubation for 15′ at 37 °C with RPMI plus 10% FCS (A) or 10% HP (B) at the indicated nanoparticle concentrations, were excised from Coomassie stained gel and analysed by LC MS/MS to identify their protein composition (see Experimental for details). Silver stained samples are shown in parallel for comparison. Positive hits (polypeptide with at least 2 significant matches, $p < 0.05$) are listed in the table, with their molar% within the same band, based on emPAI, reported in brackets. The main proteins are indicated in bold; asterisks indicate non-specific bands from FCS and HP mock controls (no NPs). M: standard molecular weight. Abbreviation used: α- 2MG: alpha-2 macroglobulin; Apo A-I/A-II/B-100/E: apolipoprotein A-I/A-II/B-100/E; BSA: bovine serum albumin; Cf-XII: coagulation factor XII; C1q-A,B,C: complement C1q subunit A,B,C; Fh: complement factor H; Fibr: fibrinogen; GSN: gelsolin; Hbf α/β: foetal haemoglobin; HRG: histidine rich glycoprotein; Ig: immunoglobulins; ITG-α2: integrin alpha; ITIH4: inter-alpha-trypsin inhibitor heavy chain H4; Kin-1: kininogen-1; KLK: Kallikrein; LBP: lipopolysaccharide-binding protein; PLG: plasminogen; SAA-4: serum amyloid A-4 protein; Sel-P: selenoprotein-P; SERPINA5: plasma serine protease inhibitor; SERPING1: plasma protease C1 inhibitor; VTN: vitronectin.

(Fig. S4, S5A and Table S3†). After subtraction of the plasma background, mock run in the absence of NPs (some of the proteins found in the NP samples were indeed totally – Fibr and HSA – or in part – Ig and Apo A-I/HDL – due to the background from plasma) and band analysis by LC MS/MS experiments confirmed that even under the more physiological conditions of ~100% HP, a major band made prevalently by HRG is predominant both at 37 °C and 4 °C. However, Kin-1 tended to decrease compared to the amount found in 10% HP while minor amounts of the IgG isotypes, F-XI and other polypeptides are identified in samples (Table S3†).

In other controls we also compared our NP-corona isolation and washing procedure with the one recently developed by Tenzer *et al.*,[12] involving a direct layering of the NPs after incubation with HP on a sucrose cushion to ensure effective separation from unbound plasma proteins. Even with this procedure, the pattern of the proteins specifically associated with the NP corona at both 10% and 100% HP was still largely characterized by the presence of HRG as the major constituent at both 37 °C and 4 °C (see ESI methods and Fig. S4†).

A similar composition, characterized by the prevalence of HRG, was also found after incubation of the nanoparticles with mouse plasma. In this medium, there are two peculiarities compared to HP: the additional presence of a high level of haemoglobin, due to the higher haemolysis characterizing the sampling of this fluid and, more interestingly, the still high prevalence of HRG even at high NP concentrations, suggesting the presence of a higher level of this protein in MP (Fig. S2D, S5B and Table S4†).

Having identified the major proteins of the SiO_2-NP corona, we performed a quantitative SDS-PAGE analysis to determine by an independent methodology their absolute amount per particle. This was achieved by calibrating the staining intensity of the most prominent bands, using standard purified proteins corresponding to their major components based on label-free MS analysis, after loading the same known amount of NPs per lane. Data confirmed the above described picture and provided other consistent information (Fig. 4 and S6†). In fact, the major ~60 kDa and ~220 kDa bands, identified as principally formed by HRG and Fibr, were indeed found to have the same electrophoretic mobility as purified human HRG and Fibr. This further supports that indeed these two proteins form the bulk of these two bands, as suggested by label-free methods. Again in agreement with label-free quantification, this quantification also showed that Kin-1 is the second major component of the hard corona at low NP concentrations besides HRG (although in a smaller proportion: HRG : Kin-1 ratio = 2.9 by quantitative densitometry, while 1.4 when using emPAI). Also in this analysis, as the nanoparticle amount increased, HRG and Kin-1 sensibly decreased while Fibr and other proteins increased. More in detail, we could determine that below 40 μg ml^{-1} concentration a single NP has a corona formed by about 19–20 HRG, 5–7 Kin-1, and 2–3 Fibr molecules (sum: 26–30 molecules). These numbers change to 8 HRG, 3 Kin-1 and 6 Fibr (sum: 17 molecules) at 80 μg ml^{-1} NPs and to about 1 HRG, 1 Kin-1 and 10 Fibr (sum: 12 molecules) at 160 μg ml^{-1} NPs. Such figures allow the estimation of footprint values of about 50 nm^2 for HRG (64 kDa) and Kin-1 (70 kDa) and 170 nm^2 for Fibr (340 kDa), which are in good agreement with the proteins' molecular weights and hydrodynamic diameters (see infra). This peculiar switch in the protein corona from a HRG-rich composition to a Fibr-rich one, depending on the NP dose (in 10% HP), was validated by western blot analysis using specific antibodies. Once again the HRG signal decreased with the NP increase, while HDL (Apo A-I) and, much strongly, Fibr increased above 40 mg ml^{-1} NPs.

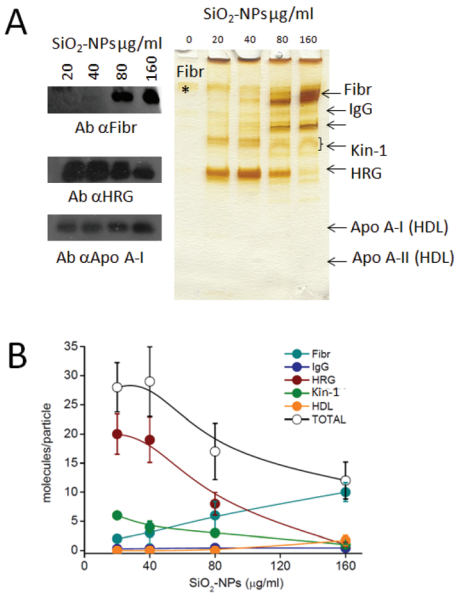

Fig. 4 Absolute quantification of the main protein composing of the HP-derived hard corona of SiO_2-NPs as a function of nanoparticle concentration. (A) Representative SDS-PAGE analysis, out of five, showing the changes of the pattern of the major proteins bound to SiO_2-NPs (the same quantity of NPs: 13 μg per lane), as a function of nanoparticle concentration during incubation for 15 min in 10% HP at 37 °C. Different from the gels of Fig. 2, where increasing amounts of NPs were analysed, here decreasing sample volumes were loaded per lane to ensure the comparison of equal NP quantities (13 μg per lane). The presence of fibrinogen, histidine rich glycoprotein and Apo A-I was confirmed by western blot analysis using specific antibodies (left panels) (B) The amounts of the main human plasma protein molecules per particle unit were calculated, after densitometry of the corresponding bands and comparison with titration curves made in parallel in the same SDS-PAGE gel with purified human protein standards (see Fig. S6A† and relative legends). The obtained molecular composition of the hard-corona is reported as a function of NP concentration; values are means ± SE (N = 5). Lines have been depicted to guide the eye.

In summary, considering the three independent pieces of evidence collected, at low NP doses, which better simulate the situation occurring *in vivo*, HRG and Kin-1 appear the most represented proteins on NPs, forming a coat of about 30 proteins with a molar ratio around 3 : 1. The concentrations of these two proteins in the culture media are relatively low, namely 15 and 8 μg ml^{-1} respectively for HRG and Kin-1. It is hence expected that when these first two proteins are depleted from the solution by increasing the NP dose, they undergo

surface-dilution leaving space available for the recruitment of other proteins, in particular fibrinogen.

Affinity of HRG and other major plasma proteins for SiO_2-NPs

The above data indicate that, in conditions of nanoparticle surface limitation (NP concentration <40 μg ml^{-1}), HRG and Kin-1 (~15 and ~8 μg ml^{-1} in 10% HP, respectively) prevent the binding of more concentrated proteins like HSA (~5–6 mg ml^{-1} in 10% HP), Fibr (~300 μg ml^{-1} in 10% HP), and IgG (~700 μg ml^{-1} in 10% HP). This indicates that HRG and Kin-1 should have a significantly higher affinity for the negatively charged silica surface than other plasma proteins. Such a prediction was confirmed by measuring the affinity of the purified HRG, Kin-1, fibrinogen and HSA for SiO_2-NPs. Experiments were performed by measuring the amount of residual free protein at equilibrium after elimination of the particle–protein complexes by ultracentrifugation and fitting the bound *versus* free protein data with the one site equilibrium equation (see Experimental) (Fig. 5). We found that the dissociation constant (K_d) of the HRG–NP complex was 2.4 ± 1.1 nM and that the maximal binding capability of a single particle was 30 ± 2 molecules per particle, a value in very good agreement with that obtained by gel quantification in HP. As expected, the affinity of Kin-1 was similar to that of HRG (4.6 ± 1.3 nM) while that of Fibr and in particular of HSA were smaller (28 nM ± 12 and >1 μM respectively). Notably, in agreement with our data, two recent studies[35,36] show that relatively high K_d values (37 ± 12 μM and 0.3–6 μM respectively) characterise the binding of HSA to variously modified negatively charged QDs.

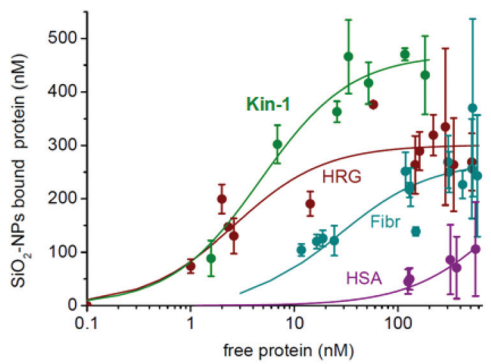

Protein	K_d (nM)	B_{max} (mol/par)
HRG	2.4 ± 1.1	30 ± 2
Kin-1	4.6± 1.3	47 ±2
Fibr	28 ± 12	27± 3
HSA	> 1000	n.d.

Fig. 5 Estimation of the affinity of HRG, Kin-1, Fibr and HSA for SiO_2-NPs. SiO_2-NPs (100 μg ml^{-1}; ~10 nM) were incubated for 15 minutes at 37 °C with increasing amounts of the indicated proteins in RPMI 1640. After separation of NPs by ultracentrifugation, the concentration of free proteins left in the supernatants was measured by the Bradford assay and plotted against SiO_2-NPs bound proteins, deduced by subtracting free protein from total protein (measured by running mock samples in which the proteins were incubated without NPs and centrifuged in parallel). Data were subjected to non-linear fitting (N = 3 for each protein). Dissociation constant (K_d) and the maximal binding capacity (B_{max}, the number of protein molecules per NP), calculated for each protein using a one-site equilibrium equation (see Experimental), are summarized in the lower table.

Moreover, the found K_d values for Fibr and HSA association with our SiO_2-NPs (28 and >1000 nM, respectively) also fit with those obtained by Pelaz *et al.*[37] (30 and 1000–4100 nM, respectively) with negatively charged FePt particles variously coated with PMA and PEG, in spite of the different chemical nature of the NPs used.

Effect of plasma proteins and of their selective lack in SiO_2-NP dispersion

Additional interesting information on the specific contribution of the investigated protein properties to the HP-hard corona on SiO_2-NPs was obtained by measuring their ability to induce nanoparticle aggregation *via* dynamic light scattering analysis. The presence of a large excess of proteins with a size comparable to, or larger than, our NPs prevents the possibility of detecting the corona coated nanoparticles and of measuring their *Z*-potential by DLS under the conditions used. Nevertheless, the formation of large protein–nanoparticle aggregates can be detected. When the nanoparticles were incubated at 20 μg mL^{-1} with 10% FCS, MP, HP, and the *corona mix*, a mixture made of the main HP corona proteins (see infra), they did not produce any observable particle aggregation (Fig. 6). Also the selective lack of each of the single protein, including HRG, in the corona mix did not induce NP aggregation (Fig. S7A†). On the other hand, when the concentration of the nanoparticles was increased above 100 μg mL^{-1}, the formation of aggregates having a hydrodynamic radius of about 100 nm was observed (Fig. S7B†) in FCS, HP, and corona mix but not in MP.

When the single proteins were analysed, we found that incubation of HRG (having a hydrodynamic diameter around 10 nm in DLS analysis) with nanoparticles induces the formation of objects with a mean diameter around 50 nm and a *Z*-potential of −9.5 mV. Such figures are compatible with the formation of a negatively charged corona of HRG molecules (the isoelectric point of HRG is 5.9–6.2) assembled around monodisperse NPs. Similar results were obtained for Kin-1.

IgG and VLDL induced extensive nanoparticle aggregation having an apparent diameter above 1 μM and between 250 and 350 nm respectively. Fibr and LDL determined only a small subpopulation of aggregated NPs. HSA and HDL did not induce NP aggregation.

Consistent with its high affinity interaction with the NPs, addition of HRG prevented the aggregation of SiO_2-NPs induced by IgG, VLDL, Fibr and LDL and, as expected, did not modify the already absent aggregation of NPs incubated with HSA, Kin-1 and HDL. These data suggest that, in the absence of HRG, other proteins can prevent particle agglomeration but also further support that HRG can compete with more abun-

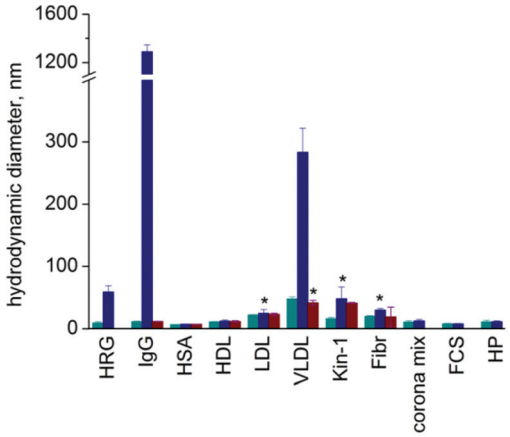

Fig. 6 Effect of plasma proteins on SiO_2-NP aggregation. DLS analysis (PBS buffer pH 7.4, 37 °C) of the single purified plasma proteins indicated at the concentration found in 10% HP, the total protein mixture of them (corona mix), 10% FCS and 10% HP alone (green bars) or after incubation (10 minutes) with 20 μg ml^{-1} SiO_2-NPs in the absence (blue bars) or in the presence (brown bars) of purified HRG (15 μg mL^{-1}). Protein concentrations: HRG (15 μg ml^{-1}), Kin-1 (8 μg ml^{-1}), HDL (150 μg ml^{-1}), LDL (78 μg ml^{-1}), VLDL (12 μg ml^{-1}), HSA (5 mg ml^{-1}), IgG (700 μg ml^{-1}) and Fibr (300 μg ml^{-1}). Secondary populations of NPs/protein aggregates (always below 5%) are indicated, when present, by an asterisk. Data are means ± SE (N = 3). Note that for high protein concentrations, corona coated silica nanoparticles cannot be detected due to the prevalent scattering by excess free proteins (see the Experimental section).

dant plasma proteins, such as IgG and VLDL, for the NP surface, inhibiting in this case their aggregation.

From this point of view it may be interesting to note that when SiO_2-NPs are incubated with mouse plasma well above the concentration of 100 μg ml^{-1} no protein aggregation is induced (Fig. S7B†). This finding is in perfect agreement with the observation that in this medium HRG remains the major corona component even at high NP doses, different from what is found in human plasma (Fig. S5D†). Altogether, these data support the idea that HRG forms a stable and quite homogeneous corona and suggest that it may be more concentrated in the mouse blood (similarly to rabbits) than in the human blood, and that, for this reason, its protective effect against aggregation is exerted at higher nanoparticle concentrations.

Different intrinsic efficacies of the main plasma proteins found in the HP hard corona of SiO_2-NPs to modulate nanoparticle cell binding

The main information provided by all the above experiments is that, apparently, a relatively small group of proteins accounts for the major features of the HP-derived protein hard-corona of SiO_2-NPs. However, we also noticed that many among the corona polypeptides identified are apolipoproteins.[38–40] Apo B-100 is found as the major component in the proteome of VLDL (Very Low Density Lipoprotein) and LDL (Low Density Lipoprotein), but it is also found as minor component of the HDL (High Density Lipoprotein) proteome; Apo A-I is the major apolipoprotein of HDL, but can be significantly found in VLDL and in LDL; Apo A-II is the second mostly represented protein in HDL, but is also detected in VLDL and LDL proteomes; Apo A-IV can be found in HDL, LDL and VLDL proteomes; Apo C-III is present in VLDL as a major protein, while in LDL as the minor ones, but it is also found in HDL; SAA-4 is similarly found in HDL, LDL and VLDL proteomes. In addition, small amounts of fibrinogen are found in HDL, LDL and VLDL. For this reason, the above indicated markers strongly suggest the involvement of all the three kinds of human plasma lipoprotein classes in the corona of SiO_2-NPs at high nanoparticle doses.

To study in more detail the role of the major human plasma proteins involved in the formation of the corona on SiO_2-NPs, the purified human HDL, LDL and VLDL fractions were therefore mixed with the purified human plasma IgG fraction (including the four human subclasses of IgG1, IgG2, IgG3 IgG4), HRG, Kin-1, Fibr and HSA at concentrations resembling the mean values present in 10% HP to obtain a simplified protein medium that will be named the corona mix for the rest of the study.

The analysis of the composition of the corona formed upon incubation of the nanoparticles with the corona mix revealed a polypeptide composition very similar to that observed when HP is used (Fig. 7A and S8A†). Moreover, uptake experiments with macrophages demonstrated that the protective effect of HP, at low nanoparticle concentrations, is maintained to a similar extent when the corona mix is used as the protein source (Fig. S8C†). Both these results confirm that the proteins selected in the corona mix are the relevant actors at play in the corona formation and in the nanoparticle–macrophage interaction.

In line with the above measured affinities, the selective lack of HRG in the corona mix, at 20 μg ml^{-1} nanoparticle concentration, resulted in an improved recruitment of the homologous Kin-1 on NPs (Fig. 7B and S8B†). On the contrary, the lack of all other proteins did not significantly modify the corona composition, which continued to be mostly characterized by a high HRG prevalence.

The ability of the corona mix to reproduce the effect of HP on the nanoparticle behaviour allowed the systematic analysis of the intrinsic ability of each protein to modulate the association of SiO_2-NPs with lymphocytes, monocytes and macrophages. When each protein was tested separately, distinctive differences were found in the three cell types (Fig. 8A). In the case of lymphocytes, any protein decreased SiO_2-NPs' cell-association. In detail, HSA, IgG and Fibr strongly diminished NP binding (75–80% inhibition) while lipoproteins (HDL, LDL, VLDL), HRG and Kin-1 determined an almost complete block of NP binding. In monocytes, Fibr slightly stimulated NPs' cell binding, IgG and VLDL had no significant effect and HSA and LDL were partially inhibitory (80–90% inhibition). On the other hand, HDL, HRG and Kin-1 decreased the binding of NPs to monocytes to values smaller than that induced by FCS and similar to HP. Finally, the most peculiar situation was observed in macrophages, where only HRG could inhibit NPs'

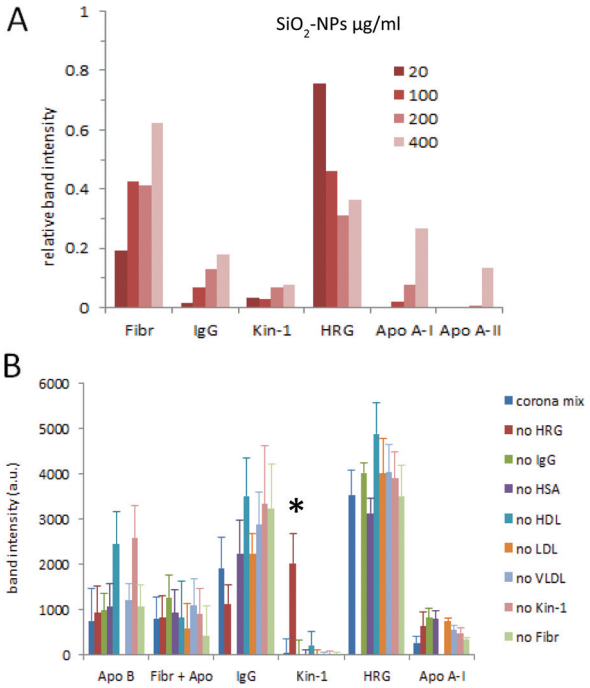

Fig. 7 Analysis of the protein hard-corona composition of SiO_2-NPs in the presence of different combinations of purified plasma proteins. (A) Composition of the corona formed around SiO_2-NPs incubated at the indicated concentrations in a RPMI 1640 medium characterized by the contemporaneous presence of HRG (15 µg ml^{-1}), Kin-1 (8 µg ml^{-1}), HDL (150 µg ml^{-1}), LDL (78 µg ml^{-1}), VLDL (12 µg ml^{-1}), HSA (5 mg ml^{-1}), IgG (700 µg ml^{-1}) and Fibr (300 µg ml^{-1}) at concentrations fairly mimicking those found in 10% HP (corona mix). Histograms show the semi-quantitative estimation of the amount of the indicated proteins associated with NPs obtained by densitometry of the corresponding SDS-PAGE bands after silver staining following normalization over the sum of the intensities of all the bands of the corresponding run (see Fig. S8A†). (B) Composition of the coronas formed after incubation of SiO_2-NPs (20 µg ml^{-1}) in the presence of the complete corona mix as above or in the presence of the corona mix lacking a single protein of the mixture as indicated. Histograms are the means ± SE of four different experiments. Representative gels out of eight are shown in Fig. S8A and B.† * significance $p < 0.05$ with respect to corona mix samples.

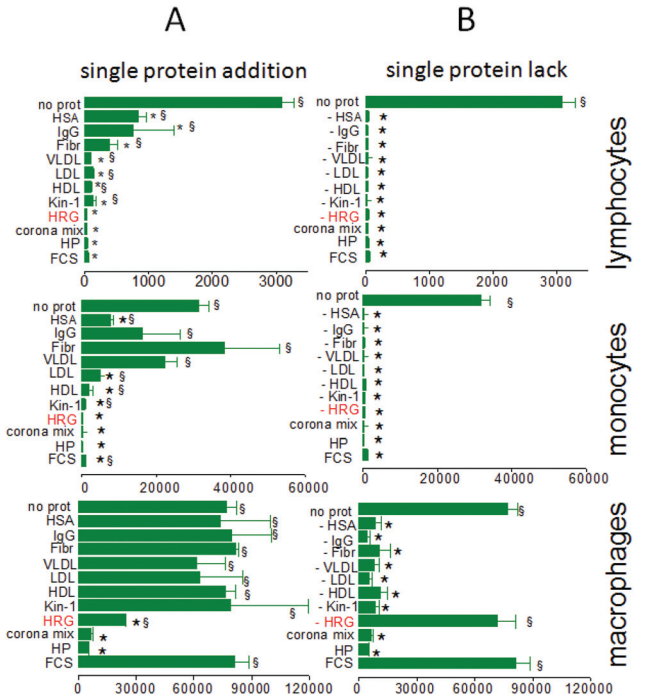

Fig. 8 Effect of the main HP-derived corona proteins on SiO_2-NP capture by lymphocytes, monocytes and macrophages. (A) Cells were incubated at 37 °C with 20 µg ml^{-1} SiO_2-NPs in RPMI 1640 without protein (no prot.), plus 10% HP (HP), 10% FCS (FCS) or the indicated purified human plasma proteins alone or all together (corona mix) at concentrations found in 10% HP as already specified in the legends of Fig. 6 and 7. After 3 h, cells were analysed by flow-cytofluorimetry to quantify NP–cell association (MFI). (B) The same analysis was performed, in parallel, incubating cells and NPs in the presence of the corona mix with the selective lack of each forming protein, as indicated (–protein). Data are the mean ± SE of duplicate experiments ($N = 3$). * significance ($p < 0.05$) with respect to no protein; § significance ($p < 0.05$) with respect to HP.

cell association (80% inhibition) and none of the other proteins, including the homologous Kin-1, had a significant inhibitory effect. Dose response analysis confirmed that these inhibitory effects are maintained in the 5–40 µg ml^{-1} SiO_2-NP concentration interval (Fig. S9†).

The above experiments indicate that, while several plasma proteins may potentially inhibit NP uptake by lymphocytes and monocytes, only HRG seems to account for the observed inhibitory effect of HP on macrophages. To further investigate this hypothesis, we incubated the cells in the presence of the whole corona mix and tested the effect determined by the selective omission of a single protein from the mixture (Fig. 8B). This experiment measures the real contribution of a given protein in the presence of the other major ones, taking into account all the reciprocal protein–protein competition and interactions that may be crucial to determine the final functional outcome. The results obtained again showed a peculiar distinction of macrophages from the other two cell types and confirmed the specific protective effect of HRG. In lymphocytes and monocytes the lack of each single protein never reverted significantly the cell binding inhibition observed in the presence of the corona mix. On the contrary, in macrophages a complete recovery of the NPs' cell association was only obtained when HRG was omitted from the corona mix.

To ascertain what step of cell association is inhibited by HRG, *i.e.* the surface binding or the subsequent cellular endocytosis, we performed experiments in which macrophages were incubated with SiO_2-NPs in no protein, FCS, HP and purified HRG after energy depletion or at 4 °C, two conditions that allow plasma membrane binding but block endocytosis. FACS analysis showed that both HP and HRG inhibited cell association when internalization was blocked, while FCS was not or less inhibitory under the same conditions (Fig. 9). This result proves that the diminished macrophage accumulation of NPs in the presence of HP and HRG is due to the hampering of cell

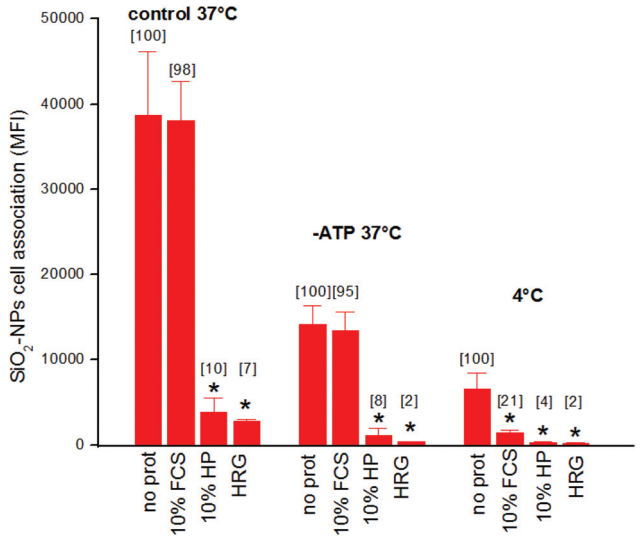

Fig. 9 Effect of energy depletion and low temperatures on the SiO_2-NPs' association with macrophages. Macrophages were pre-treated or not for 30′ at 37 °C with sodium azide 10 mM plus 2-DOG 5 mM to deplete ATP (-ATP) in the presence of RPMI 1640 without protein (no prot.), with 10% FCS, 10% HP or 15 μg ml^{-1} HRG (corresponding to its concentration in 10% HP). Then, SiO_2-NPs 20 μg ml^{-1} were added for 2 hours both at 37 °C or 4 °C. After incubation, the cells were washed and analysed by using a flow-cytometer to quantify NP–cell association (MFI). Data are the mean ± SE of three experiments run in duplicate. Numbers in brackets and * are % and significance ($p < 0.05$) with respect to no prot samples under each condition.

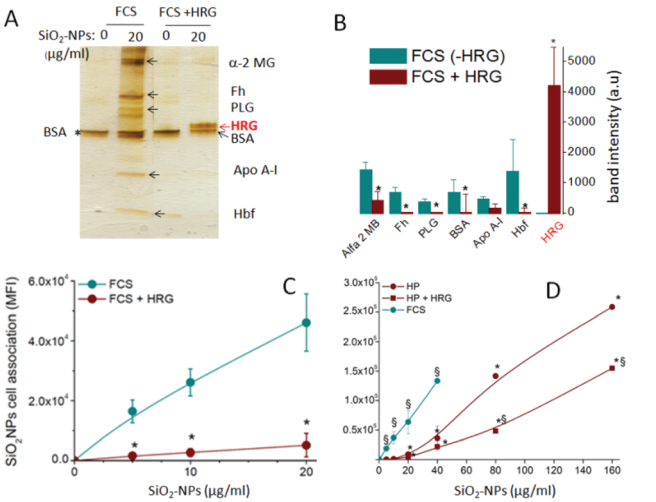

Fig. 10 Effect of HRG on the capture of SiO_2-NPs by macrophages in FCS and HP. (A) SiO_2-NPs (20 μg ml^{-1}) were incubated with 10% FCS or with 10% FCS plus purified human HRG (15 μg ml^{-1}) for 15 minutes at 37 °C, and the hard-corona was analysed by SDS-PAGE after particle recovery and washing by ultracentrifugation (a representative gel out of three is shown). The single bands corresponding to the indicated major proteins, validated by MS, were quantified by densitometry after silver staining, as reported in panel (B). BSA non-specific signal, marked in mock (no NPs) SDS-PAGE samples is indicated by an asterisk in the gel. Data are means ± SE ($N = 3$). * significance ($p < 0.05$) compared to HRG lacking conditions. (C and D) Macrophages were incubated with SiO_2-NPs at the indicated doses in RPMI with 10% FCS and 10% FCS + 15 μg ml^{-1} HRG (C) or in 10% FCS, 10% HP and 10% HP + 15 μg ml^{-1} HRG (D) for 3 h at 37 °C. NPs' association with cells was determined after washing by flow-cytofluorimetry. Data are the mean ± SE of three experiments run in duplicate. * significance ($p < 0.05$) compared to FCS; § significance ($p < 0.05$) compared to HP.

surface binding, which in turn affects the following active endocytosis of the particles.

SiO_2-NPs are well known to induce cytotoxicity and cytokine release.[23,24] No cell death and production of IL-1β were observed in parallel experiments in which cells were treated with SiO_2-NPs for 3 hours in the presence of different protein mixtures as above. However, after a prolonged incubation (24 h), we could evaluate the modulatory effect of the various plasma proteins involved in the formation of the HP corona on the intrinsic efficacy of bare NPs to kill cells and to induce IL-1β. The different proteins of the corona mix protected cells with different efficacy and selectivity, when used as single agonists: VLDL, LDL, HDL, Kin-1 and HRG are strongly protective in both monocytes and macrophages while HSA, IgG and Fibr are poorly protective in monocytes and protective in macrophages. Consequently, FCS, HP and the corona mix all completely inhibited the cytotoxic and pro-inflammatory effects of SiO_2-NPs, and in no case the selective deprivation of single proteins from the corona mix resulted in the recovery of cytokine production and cell toxicity (Fig. S10†). These data suggest that, at least at the relatively low NP dose used in this study, a specific protein corona composition is not required to block the toxic and proinflammatory effects of SiO_2-NPs and that many different proteins can ensure non-specific protection of the membrane-active silica surface of NPs.

If HRG is the protein responsible for the protective effect of HP toward macrophage uptake, when it is predominantly present in the corona, its absence in FCS may explain the effective capture of SiO_2-NPs by macrophages in this medium. Consequently, we decided to test the effect of the addition of human HRG to FCS at a concentration equivalent to that present in HP. Regarding the corona composition, an almost total displacement of FCS-derived typical proteins (α2-macroglobulin, Apo A-I, haemoglobin α/β) was observed and HRG became the major protein as in HP (Fig. 10A and B). Consistently, a strong reduction of NP capture by macrophages in FCS implemented with HRG was observed (Fig. 10C). Also the addition of purified HRG (+30 μg ml^{-1}) to HP determined a further improved reduction of SiO_2-NPs' macrophage capture (Fig. 10D). Moreover, HRG indeed completely restored the ability of HRG/Kin-1 depleted HP to inhibit NPs' macrophage capture (Fig. 11C). Other control experiments in which NPs were incubated with macrophages in the presence of plasma depleted of Fibr, a major protein present in the corona after HRG, showed no significant variation of HRG content in the corona and a conserved ability to inhibit the NPs' capture by cells (Fig. S11†). Another interesting aspect of this control is the lack of Kin-1 in the corona, likely due to its involvement in the coagulation process and possible loss in fibrin clots. This observation further confirms the irrelevant contribution of

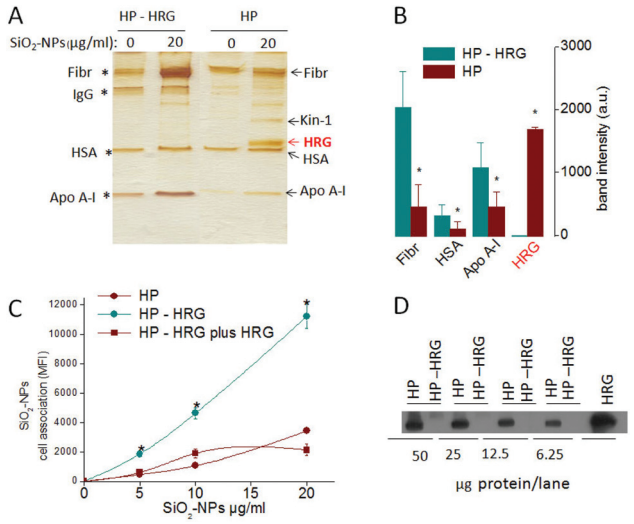

Fig. 11 Effect of HRG depletion on the ability of HP to inhibit SiO_2-NPs' capture by macrophages. (A) SiO_2-NPs (20 μg ml^{-1}) were incubated with normal (HP) or HRG-depleted 10% HP (HP−HRG) for 15 min at 37 °C. The hard-corona was analysed by SDS-PAGE (representative of three) after particles washing by ultracentrifugation and the main proteins (indicated by arrows and validated by MS) were quantified by densitometry after silver staining. Non-specifically recovered proteins (Fibr, IgG, HSA, Apo A-I) from mock (no NPs) samples run in parallel are marked by asterisks in the gel. (B) Histograms represent the band intensity of indicated proteins and are the mean of three experiments ± SE. * significance ($p < 0.05$) compared to HRG lacking conditions. (C) Macrophages were incubated at 37 °C for 3 h with SiO_2-NPs at the indicated doses in the presence of RPMI 1640 medium plus 10% HP, 10% HRG-depleted HP or 10% HRG-depleted HP re-integrated with HRG 15 μg ml^{-1}, and NPs' association with cells was determined after washing by flow-cytofluorimetry. Data are the mean ± SE of three experiments run in duplicate. * significance ($p < 0.05$) compared to a medium containing HRG. (D) The removal of HRG from HP was validated by western blotting by loading on a 12% non-reducing SDS page 50, 25, 12.5 or 6.25 μg of HP and HP−HRG (previously analysed for total protein concentration by the Bradford assay) and 0.675 μg of purified HRG as the positive control. The blot was developed using the ECL system for 10 seconds.

Kin-1 to the ability of plasma to inhibit SiO_2-NPs' capture by macrophages.

Discussion

In this study we found further evidence strongly supporting the paradigm that the composition of the protein corona is one of the main factors that control the interaction of nanoparticles with cells. We were however interested not only in elucidating the effect of the corona on the nanoparticle biological activity, but also in understanding which are the relevant *in vitro* conditions required to gain information predictive of the behaviour of the nanoparticles *in vivo*. The initial idea that prompted this investigation was that the nanoparticles, once injected in the bloodstream, will experience a substantial dilution and will accumulate primarily in the cells deputed to capture foreign entities. Consequently, we focused our attention on: human plasma, low nanoparticle concentrations and phagocytic cells.

In line with such premises and with previous studies,[21,27,41] we found that the protein hard-corona undergoes dramatic composition changes depending on the protein source selected (FCS or HP). Moreover, we here show that also the nanoparticle concentration is a determinant parameter, as we will discuss in detail later. We identified two groups of 7 and 12 proteins respectively as major constituents of FCS and HP derived coronas. Among them, only Apo A-I, Apo A-II (HDL markers) and albumin (HSA or BSA) are present in both the sets. When only the most represented proteins were analysed, which are α2-macroglobulin and haemoglobin α/β for FCS and HRG, Kin-1, and Fibr for HP, no overlap is found between the coronas formed in the two media. Strikingly, in FCS, not only Fibr and Kin-1 are not present, due to the involvement of these two proteins in clot formation which is part of the production of such medium, but also HRG is missing. Such absence likely leaves room to other proteins on the NPs whose affinity for the silica surface is lower. This is confirmed by the fact that, when HRG is added to FCS, the corona composition changes completely and becomes similar to that formed in HP.

Such a relatively simple composition of the nanoparticle corona may appear in contrast to other reports, where much larger numbers of corona forming polypeptides are identified.[2,3,5,11–13,27,34] However, this disagreement can be in part explained by our choice to focus on abundant corona components, present in stoichiometric ratios, based on the conceivable hypothesis that these are the molecules predominantly influencing the nanoparticles' biological behaviour.

Second, in some cases, we aimed at identifying protein families (Ig, lipoproteins) using bona fide and well recognized markers, without differentiating all single composing polypeptides or searching for minor proteome components. For example, Apo A-I allowed us to identify the presence of HDL in the corona[9] in spite of the larger polypeptides' set that characterizes these lipoproteins. In fact, the lipoprotein proteome is formed by at least 40 polypeptides, in part overlapping with the highly heterogeneous coronas recently reported on Au- and SiO_2-NPs.[5,11,12,38–40] This suggests that the reported complexity of the NP corona in shotgun experiments, especially for the abundant sub-stoichiometric components, may be due, at least in part, to the contribution of the HDL, LDL and VLDL proteomes. Another similar case is represented by antibodies: we marked them as IgGs in our study but several polypeptides or virtual polypeptides, generally reported in shotgun proteomics experiments, contribute to the formation of single antibody molecules and to different isotypes (that were indeed identified by us in the corona).

Eventually, special consideration deserves the fact that we performed our experiments at low nanoparticle concentrations: under these highly limiting conditions, only the proteins with the highest affinity for the nanoparticle surface are supposed to effectively bind them, and this is reasonably expected to simplify the corona protein pattern. Indeed, we

found that at higher NP concentrations, both the absolute number of protein bands in SDS-PAGE analysis and their heterogeneity sensibly increased, in line with other studies.[2,11,13,42] Such observation is in agreement with our conclusion that the depletion of HRG allows the recruitment of other proteins in the corona. In this respect, it may also be important to note that, at higher NP doses, the simple notion of neat hard coronas around individual NPs may not be apt to interpret data. In fact, in line with another study,[27] NP/ plasma protein large aggregates form above 100 μg ml^{-1} NP concentrations (Fig. S4†). This process may lead to non-specific recovery of more plasma components by NP clusters, either in solution or during the centrifugation step (*entrapment effect*). Moreover, the concept of corona under these conditions may not be useful, especially when proteins of the same size as or bigger than the NPs are found, while a heteroaggregation model may be more appropriate.[43]

A further element to take in consideration is the results obtained by biochemical titration of the maximal amount of protein units which can associate with NPs. In our study we determined, using purified proteins, that the maximal number of proteins that can accommodate on the surface of our 26 nm diameter SiO_2-NPs is about 30 for HRG, 47 for Kin-1 and 27 for Fibr. These data are in line with the quantification of the same proteins in the corona when particles are incubated with HP at low NP doses (20 HRG plus 7 Kin-1 and 2–3 Fibr, corresponding to 30 total protein molecules). Not only such experimental figures are in agreement with geometric considerations, providing acceptable protein footprints, but they are also in line with previous literature reports. Dell'Orco *et al.*,[44] based on geometric simulations, estimated the maximal number of HSA (8 nm diameter), HDL (10 nm diameter) and Fibr (16 nm diameter) molecules that can form a corona monolayer around 70 nm diameter co-polymer NPs. Normalizing their estimate for the difference in surface (~7 times larger compared with our 26 nm diameter SiO_2-NPs) a maximal number of 54 HSA, or 37 HDL, or 16 Fibr molecules per particle can be calculated, not far from our estimations. At the end, it becomes quite evident, both on the basis of geometry and of the above discussed results, that tens of protein units per particle, and not hundreds, form a corona monolayer around ~26 nm diameter NPs.

This having been specified, we must stress that although other proteins co-migrating with the major protein bands identified were indeed detected by MS (see Table S2†) their scores and semi-quantitative label-free estimation (emPAI parameter)[32] indicated that they are minor components with respect to the major ones, especially at low NP concentrations. This tendency was indeed confirmed using various temperatures (37 °C *vs.* 4 °C), HP percentages (10% *vs.* 100%) and centrifugation protocols for isolating NP-corona complexes.

Taking into account all above considerations and evidence, we conclude that the most peculiar distinctive feature of the HP corona (and also of the MP corona) of silica nanoparticles is the prevalent presence of Histidine-Rich Glycoprotein (HRG) under low nanoparticle concentration conditions (that are likely more representative of *in vivo* situation). With some differences, possibly due to the use of higher nanoparticle doses and different conditions, this observation is in agreement with those obtained by Monopoli *et al.* studying silica nanoparticles.[45] Indeed, in experiments in which much larger SiO_2-NP concentrations were tested (mg ml^{-1} range), these authors found that the HP-derived corona is composed by several proteins including Fibr as the major protein but also HRG, Kin-1, IgGs, HSA, PLG and several HDL and LDL markers. Moreover, increasing the plasma concentration from 10% to >55% changed this pattern in such a way that HRG became the major corona protein, followed by Fibr and HSA, a result compatible with our data. It is also to be noted that HRG and Kin-1 were found as major corona components also in the HP corona of negatively charged NPs made of PLGA[46] and dextran-iron oxide.[47] Such observations suggest that HRG and Kin-1 may have a high affinity for negatively charged surfaces. In the case of our silica nanoparticles, this hypothesis is supported by the nanomolar dissociation constants we measured.

It is also worth stressing that we always consistently observed a relatively poor abundance of serum albumin under any condition tested (HP at both 10 and 100% concentration, HS, FCS and MP), often accounted just by the background residue, in spite of the fact that this protein is the most abundant in plasma/serum and has been reported as the major component of the hard corona in SiO_2-NPs and other NPs. The low affinity of HSA for amorphous silica (>1 μM), similarly seen in other negatively charged nanoparticles,[36,37] is consistent with this finding and somehow questions the inclusion of albumin in the category of hard-corona proteins for SiO_2-NPs, and possibly other negative NPs, where its presence may be due to the incomplete washing of the abundant free protein.

The above discussed biochemical abundance of HRG in the SiO_2-NP corona is sound also because it is consistent with the main functional observation made in this study, namely that HRG was proven to have an intrinsic ability to inhibit the capture of these NPs by macrophages, while several other plasma proteins variously found in the corona have not. HRG abundance simply explains the here shown ability of human plasma to decrease the macrophage capture of these NPs compared to the bare ones. Indeed, the strong inhibitory action of the HP corona on the ability of macrophages to capture NPs implies that the protein(s) mediating such an effect must be present in a large amount in all nanoparticles in solutions. This suggests that, even if minor components may be present in small proportions, or at strong substoichiometric ratios as indicated by other studies,[5,12,34] they are not able to counterbalance the inhibitory effect of HRG. Such minor corona components may contribute to the interaction of SiO_2-NPs with macrophages, or other cell types, for example favouring, in a positive way, the insurgence of new properties. Still, our data point to HRG as a major functional player able to obstacle NPs binding to macrophages.

Available information on HRG further supports our structural and functional conclusion. In fact HRG, belonging to the type 3 cystatin family,[48] found in many vertebrates and invertebrates[49,50] is formed by two N-terminal cystatin-like domains, a central histidine-rich region (HRR), containing multiple GHHPH tandem repeats flanked by proline-rich regions, and a C-terminal region.[50–52] It is crucial to note, from our perspective, that the HRR is responsible for the binding of HRG to negatively charged matrixes like phospho-cellulose, heparin and heparan sulphate and for its antibacterial/antifungal activity.[53–55] Consequently, HRR could also be responsible for the here observed high affinity of HRG for the negatively charged surface of SiO_2-NPs. This hypothesis is supported by the fact that Kin-1, which is the only other type 3 cystatin that contains a HRR, has a similar high affinity for the nanoparticles, and, consequently, it is not only present in a significant amount on the SiO_2-NP surface (together with HRG) but also replaces HRG when this is removed from the corona. The other type 3 cystatins present in serum, like kininogen 2 and fetuins, which do not contain HRR, were not found associated with SiO_2-NPs under the conditions used, strongly suggesting that it is the HRR domain and not the cystatin one that mediates HRG and Kin-1 binding to SiO_2-NPs. Time course experiments show that HRG and Kin-1 are not displaced from the corona after a prolonged incubation by other plasma proteins and that these proteins remain the major corona components at low NP doses.

It can also be noted that the presence of Kin-1 fits with other known properties of SiO_2-NPs. In fact, at high NP doses, in addition to Kin-1, partially processed as testified by its anomalous electrophoretic migration, Kallikrein and coagulation factor XII (F-XII or Hageman factor) are also present among other minor corona components. These three proteins indeed form a complex called the *contact system* on negatively charged surfaces and trigger the coagulation process.[56] SERPING1, a negative regulator of F-XII, is also present in the corona as the minor constituent. These data are in agreement with functional data showing that amorphous silica can accelerate the coagulation cascade *via* the contact system.[57] Our experiments with coagulated plasma, in which not only fibrinogen but also the contact system (Kin-1, Kallikrein and F-XII) is depleted, confirm that these other minor corona components are not involved in inhibiting SiO_2-NPs' macrophage capture.

The variation of the SiO_2-NP corona composition upon dose increase, which undergoes a decrease of HRG and an increase of the other plasma proteins with lower affinities for the silica surface, is consistent with the HRG plasma concentration, with its measured affinity and maximal binding capacity for SiO_2-NPs, and with the rough geometric features of nanoparticles and proteins engaged in this interaction. The density of silica nanoparticles prepared by the Stöber method is 2.0 g ml^{-1}.[31] From this value, it is possible to estimate a surface area of 115 m^2 g^{-1} for nanoparticles with a diameter of 26 nm. Using the footprint value of 60 nm^2 estimated above for one HRG or Kin-1 molecule, it is possible to calculate that 10% HP contains enough HRG or Kin-1 to coat ~100 μg ml^{-1} of SiO_2-NPs, while HRG alone can coat a surface area corresponding to about 74 μg ml^{-1} nanoparticles. Such figures are in agreement with calculations based on the experimentally determined maximal binding capacity and affinity of our NPs for HRG (~30 molecules of HRG per particle; K_d = 2.4 nM) that predict a ~90% depletion of soluble HRG in 10% HP by 80 μg ml^{-1} NPs (see paragraph 14 of the ESI† for more details). However, in the complex mixture of HP, other proteins with lower affinity but higher concentration can compete for nanoparticle surface adsorption also before such a threshold is reached. Indeed, we found some Fibr molecules in the HP corona also at the lowest NP concentration explored (20 μg ml^{-1}). Fibr affinity for the silica nanoparticle is about 10-fold lower than that of HRG and Kin-1, but its concentration is 3–4 fold larger in molar terms. Hence, as long as the nanoparticle concentration increases it can easily adsorb onto the fraction of the nanoparticle surface no more protected by HRG and Kin-1, progressively diluting these two proteins in the corona. Eventually, at 160 μg mL^{-1} NP concentration, the corona is formed by other proteins and, if we consider the protein mass, almost exclusively by large Fibr molecules. Our data predict that other proteins will likely adsorb in a sensible amount at larger NP concentrations, when Fibr will also be depleted from the solution. Such a strong dependence of the corona composition on the nanoparticle concentration is particularly relevant because, over all the proteins tested, HRG is the only one strictly necessary to inhibit the SiO_2-NP capture by human macrophages. No other protein, including the structurally related Kin-1, is able to reduce macrophages' capture of NPs. The absence of HRG in FCS explains the different uptake behaviour observed in the two media. Remarkably, these results also show that different compositions of the corona may determine or not different interacting properties of the particles depending on the cell type. Indeed, while the nanoparticle uptake efficacies displayed by monocytes and lymphocytes are very similar in FCS and HP, only using macrophages we could detect a sensibly different uptake which correlates with the different origin of the corona. The choice of cellular model for determining the biological behaviour of nanoparticles is hence very important.

Macrophages are mainly responsible for particulate blood clearance. This selective "stealthing effect" of HRG with respect to the nanoparticle capturing ability of primary human macrophages may have important consequences in the bioavailability of SiO_2-NPs, and, possibly, other negative NPs *in vivo*.

Although the mechanistic explanation of the HRG effect will require further investigations, we can already formulate a reasonable hypothesis, based on available evidence. Experiments performed at low temperatures and upon inhibition of energy dependent processes indicate that HRG prevents the binding of the nanoparticles to the cell plasma membrane, which is the first step of internalization. We've already reported that in protein free media the silica nanoparticle binds to cell membranes displaying a relevant membrane

disruption activity.[23,24] Such a non-specific interaction could be considered responsible for the strong capture of the "naked" nanoparticles in all the cells considered. Apparently, the formation of the corona in the absence of HRG is able to prevent nanoparticles' association with other cell types with the very exception of macrophages. In this last case, nanoparticle internalization could arise from the presence of specific receptors, such as HSA, fibrinogen (MAC-1), HDL scavenger receptors, and Fc receptors capable of recognizing the nanoparticle adsorbed proteins (see the scheme in Chart 1). This hypothesis may explain why Kin-1 is not able to prevent macrophage capture like its homologous protein HRG. In fact Kin-1 also binds to the MAC-1 scavenger receptor present on these cells.

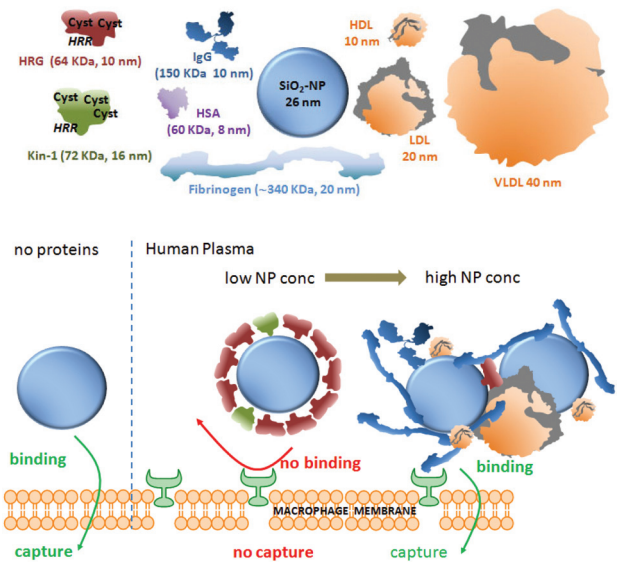

Chart 1 Upper: pictograms of the main proteins engaged in the formation of the concentration-dependent corona of silica nanoparticles in HP. The size and shape of the different proteins were roughly represented in the scale to appreciate their dimension with respect to 26 nm diameter SiO_2-NPs used in this study, also shown. Note that the indicated protein diameters are deduced by DLS measurements performed in this study and that especially in the case of fibrinogen, a fibrillary protein with a length around 40 nm, the value is apparent. The shape of HRG and Kin-1 is an artistic guess based on their secondary structure, in the absence of more detailed information, where Cyst indicates cystatin domains present at the N-terminus, while HRR is the cationic Histidine Rich Region likely responsible for the interaction with the negatively charged, silanols containing, surface of SiO_2-NPs. Lower: uptake of SiO_2-NPs in the absence of a protein corona (left) or (right) in the presence of a heterogeneous corona (Fibr, HDL, LDL and IgG major proteins here represented—note that HSA is omitted since present in a very small amount) formed at high NP concentrations (here, some degree of particle aggregation is depicted to account for DLS data). Binding and endocytosis inhibition of monodisperse NPs having a uniform HRG-rich corona formed at low NP concentrations, with a minor contribution of Kin-1 (middle). Note that the corona effects are exerted at the level of plasma membrane binding, non-specific for naked NPs or mediated by macrophagic scavenger receptors for HP coronas at high NP concentrations, which allows the subsequent energy-dependent capture of the NP (see the text for thorough discussion).

Indeed, Mac-1, an integrin heterodimeric receptor expressed on macrophages, known to bind to iC3b-coated target cells, is a multifunctional receptor able to bind also fibrinogen and the Kallikrein cleaved Kin-1 or HKa.[58]

In the case of FCS, it may be useful to note that the most abundant corona protein in this medium, haemoglobin, may bind to scavenger receptor class B type 1 (SR-B1), and CD163 expressed on macrophages.[59]

The fact that SiO_2-NP–macrophage binding and the following uptake do not occur effectively when the corona is mostly composed of HRG may indicate that these cells do not have receptors for HRG or, alternatively, that the nanoparticle adsorption may prevent the recognition of HRG, due to unfavourable orientation. Indeed, HRG was reported to mediate the capture of HRG-opsonized dead cells by monocytes, *via* the link formed by IgG_2,[60] although other pieces of evidence did not support this possibility.[61] We here observed an opposite, anti-opsonic effect of HRG on SiO_2-NPs, not modulated by the presence or the absence of IgG. It is therefore possible that the interaction of HRG with the silica surface is different from that with the dead cell surface, so that further binding of IgG_2 is impossible. Other studies showed that HRG also binds fibrinogen.[62] However, we did not find a positive correlation between HRG and Fibr recruitment in the HP corona, while, on the contrary, fibrinogen binding occurred after the consumption of free HRG at higher NP doses. Once again, it may be that the ability of HRG to bind Fibr is compromised in silica-adsorbed HRG. A role in the ability of HRG to inhibit the binding to macrophages may also be played by its glycosylation. In fact, recent observations indicate that glycosylation of the corona associated glycoproteins, among which HRG was indeed also identified as a major constituent, not only stabilizes SiO_2-NPs in solution but also reduces the binding to macrophages,[42] in good agreement with our data, showing the high prevalence of highly glycosylated HRG in plasma excess and the parallel prevention, under these conditions, of NP aggregation and macrophage capture by this protein. However, since we have shown that the homologous and glycosylated Kin-1, although able to bind effectively to SiO_2-NPs, cannot prevent macrophage binding, it seems clear that subtler biochemical, HRG-specific, mechanisms must play a role, as discussed above.

Conclusions

In summary, we here report that a single protein, namely HRG, present in human (and mouse) plasma but not in FCS, is potentially capable of completely changing the biological fate of silica nanoparticles by strongly reducing their capture by macrophages. HRG appears to have a high affinity for the silica surface, likely arising from its histidine-rich motifs, and is able to compete for nanoparticle binding with proteins present in plasma at much higher concentrations. However, the limited plasma concentration of HRG allows for the formation of a homogeneous and stable corona only below a rela-

tively small nanoparticle concentration. Indeed, a strong assumption of our study is that the final low particle concentrations better simulate the *in vivo* situation. Low particle/high protein situations are more plausible in many cases, such as rapid injection in the bloodstream. However, it is also possible that in some circumstances, for example subcutaneous injection, or depending on the NP system nature, the initial *bolus* of NPs provides enough particles for aggregation to occur before dispersion. So, high NP dilutions and the corona formed in this case should not be taken as an *a priori* absolute requirement to predict the behaviour of NPs *in vivo*. In other cases, at least in the initial phase, low dilutions may better represent the situation *in vivo*. In this light, further experiments should be focused on the kinetics of reversion or time evolution of protein–NP complexes and aggregates initially formed at relatively high NP concentrations in a given host fluid upon subsequent dilution in the same, or other, physiological solutions. Nevertheless, our data, pointing to the phenomena linked to NP concentration relative to protein availability, still highlight how only a careful choice of experimental conditions may allow obtaining *in vitro* results predictive of the general nanoparticle biological behaviour.

In summary, three variables are essential for useful corona functional analysis: (1) the use of an appropriate physiological medium (plasma proteins for NPs envisaged for blood injection), (2) the careful selection of nanoparticle concentration and (3) the use of appropriate cell models. Interspecific differences in HRG plasma concentrations must also be taken into account, as our data obtained in mouse plasma indicate, since this might modify the pharmacokinetics of negatively charged NPs.

Eventually, the results here discussed may also disclose intriguing applications. First, HRG has been shown to regulate haemostasis and to antagonize cancer progression.[63,64] Further studies will be required to assess if such effects are retained in the NP-adsorbed HRG, and can be possibly exploited for medical purposes. Second, our data also suggest the possibility that the stable recruitment of HRG and its further stabilization on the surface of nanosystems could be used as an alternative strategy to obtain a biomimetic and biocompatible "stealthing" layer on nanotheranostics.

Experimental section

Synthesis of fluorescein-APTES (FITC-APTES)

Fluorescein isothiocyanate (0.031 mmol) was dissolved in 10 mL of dry tetrahydrofuran (THF) in a flame-dried flask. Then 7.2 μL of (3-aminopropyl)triethoxysilane (APTES, 0.031 mmol) and 4.3 μL of triethylamine (0.031 mmol) were added. The mixture was stirred for 16 h at room temperature under a N_2 atmosphere (TLC, silica plate, ethyl acetate, R_f = 0.5). The solvent was evaporated and the residue was dissolved in 3 mL of THF. This solution was added dropwise to 20 mL of *n*-hexane and the precipitated product was recovered by centrifugation (4000*g* for 5 minutes). This purification procedure was repeated two times. The product (12 mg) was obtained as yellow powder (64% yield). ESI-MS *m*/*z*: $[M + H]^+$ calcd for $C_{30}H_{35}N_2O_8SSi$, 611.2; found, 611.6 (100%).

Nanoparticle synthesis, characterization and stability

Stöber nanoparticles were prepared as follows: to a thermostated vessel charged with ethanol (20 mL), 500 μL (2.45 μmol) of 4.9 mM solution of FITC-APTES in DMSO and 100 μL (0.45 mmol) of TEOS were added under stirring at 25 °C. In order to initiate the polymerization, 1.2 mL of 7.4 M aqueous solution of ammonia were then added. After 16 hours, the solution was diluted to 80 mL with ethanol and concentrated to the original volume by ultrafiltration through a regenerated cellulose membrane (cut-off 10 kDa) under nitrogen pressure (4 bar). The procedure was repeated six times. The solution was filtered through a 0.45 μm regenerated cellulose filter to remove the precipitate. The dilution–concentration procedure was then repeated five more times with MilliQ water. The resulting solution was filtered through a 0.22 μm regenerated cellulose filter. The fluorescein concentration is determined by using its absorbance at 490 nm (ε = 77 000, pH 9.0). The nanoparticle weight is determined by weighing a dried aliquot of the product. The loading of the FITC-APTES-Si in the nanoparticles was ~0.56% (w/w). Residual free FITC in the preparations were always <0.35% (<0.25 μM) compared to the amount of FITC coupled to the NP matrix (76–99 μM), and were not found to significantly contribute to cell fluorescence in FACS experiments (see below). DLS measurements provide an average diameter of 26 ± 3 nm (number weighted) with 0.19 PDI (in phosphate-buffered saline [PBS], pH 7.4). The zeta-potential value (the same conditions as DLS analysis) is −18.3 mV. TEM analysis yields 25 ± 3 nm diameter in good agreement with the DLS size. NP batches (2 mg ml^{-1}) were stable in MilliQ water for at least 2 months.

DLS measurements

Proteins were incubated in PBS (10 mM, pH 7.4) with Stöber nanoparticles (20 μg ml^{-1}) at 37 °C for 10 minutes. Samples were then transferred into a 120 μl quartz cell and subjected to DLS analysis using Malvern Instruments Zetasizer NanoS apparatus equipped with a 633 nm laser and a Peltier thermostating system. The proteins used were histidine-rich glycoprotein (HRG, 15 μg mL^{-1}), immunoglobulins G (IgG, 700 μg mL^{-1}), human serum albumin (HSA, 5000 μg mL^{-1}), high density lipoproteins (HDL, 150 μg mL^{-1}), low density lipoproteins (LDL, 78 μg mL^{-1}), very low density lipoproteins (VLDL, 12 μg mL^{-1}), Kininogen-1 (Kin-1, 8 μg mL^{-1}), and fibrinogen (Fibr) (300 μg mL^{-1}). Prolonged incubation times did not lead to further size modification. Volume weighted distribution analyses were used in order to allow more reliable detection of nanoparticles and aggregates in the presence of a large amount of serum proteins (in number-weighted distribution analysis scattering contribution from serum is prevailing over nanoparticles at low nanoparticle concentrations, while in intensity-weighted distribution scattering from larger aggregates present in even very small amounts is predominant).

Note that the average size provided by volume weighted distributions is somewhat larger than those provided by number weighted distribution as a result of the third-power dependence of volume over radius. However, in those experiments where the protein concentration was particularly high (HSA, HDL, IgG, HP, FCS and corona mix) or where the protein size is comparable to or greater than the particle size (VLDL, LDL) the corona-coated nanoparticles, but not larger nanoparticle aggregates, resulted to be undetectable also in the volume weighted analyses. In other experiments, Stöber nanoparticles (100–500 μg ml^{-1}) were incubated with 10% v/v FCS, 10% v/v HP or 10% v/v MP diluted in PBS pH 7.4, and DLS analysis was performed as above.

Cells

Peripheral human blood cells and plasma samples (see below) utilized in this study derived from healthy blood donors, as anonymously provided by the Transfusional Center of the Hospital of Padova, in compliance with the relevant laws and institutional guidelines. Written informed consent for the possible use of these materials for research purposes was obtained from blood donors by the Transfusional Center. Data related to human samples were all analysed anonymously. Human leukocytes and plasma were not obtained consequently to experimentation on human beings but as a consequence of voluntary and informed blood donation for transfusions: no approval of the Ethics Committee is needed in such cases in our institution. Monocyte-enriched preparations were isolated from human buffy coats by centrifugation over a Ficoll-Hypaque step gradient and a subsequent Percoll gradient as described by Tavano *et al.*[65] After 1 h adherence to plastic in RPMI 1640 (Gibco, BRL see the ESI for full composition description) supplemented with 2% (v/v) FCS (Euroclone, endotoxin <0.3 EU ml^{-1}) and antibiotics (100 U ml^{-1} penicillin and 100 μg ml^{-1} streptomycin) stimuli were added. Human macrophages were derived from monocytes for 7 days with 100 ng ml^{-1} macrophage colony-stimulating factor (M-CSF, Peprotech) in RPMI 1640 plus 20% FCS. Macrophage differentiation was checked by morphological inspection and differential expression of CD14 and CD16 as previously described.[23] Human hepatocellular carcinoma HepG2 cells were maintained in RPMI 1640 medium supplemented with 10% FCS + antibiotics and split every 2–3 days. All cells were kept at 37 °C under a 5% CO_2 humidified atmosphere.

Human plasma, human serum, mouse plasma and proteins

Pooled platelet poor human plasma from healthy donors (HP) supplemented with 22% v/v of citrate phosphate dextrose adenine solution (CPDA-1) as an anticoagulant (composition, ESI†) was kindly provided by Centro Trasfusionale of the Hospital of Padua (ULSS 16), frozen in aliquots in liquid nitrogen and stored at −20 °C. Human serum (used as fibrinogen depleted plasma) was from TCS Biosciences, frozen in aliquots in liquid nitrogen and stored at −20 °C. Mouse plasma was obtained from freshly drawn mouse blood (containing 0.38% v/v sodium citrate as an anticoagulant) after centrifugation at 1800*g* for 10 minutes without an accelerator and brake and subsequent spin at 15 000*g* for 2 minutes to remove contaminant cells and debris. After freezing in liquid nitrogen, plasma aliquots were stored at −20 °C. To minimize the formation of the Fibr/Fibronectin rich protein cryoprecipitate from plasma, which forms when this is thawed at low temperatures, frozen HP and MP aliquots were thawed in a water bath at 37 °C and then brought to the desired temperatures, depending on the experiment.[66]

Histidine-rich glycoprotein (HRG) was purified from human plasma (see HRG purification). Human immunoglobulin G pool (IgG) and human albumin (HSA) were purchased from Sigma Aldrich, human high, low and very low density lipoproteins (HDL, LDL, VLDL), human High Molecular Weight Kininogen (HMWK or Kininogen 1) and human fibrinogen (Fibr) were from Calbiochem. In DLS, corona and cellular experiments, all proteins were used at concentrations corresponding to 10% (v/v) human plasma: HRG 15 μg ml^{-1}; IgG 700 μg ml^{-1}; HSA 5 mg ml^{-1}; HDL 150 μg ml^{-1}; LDL 78 μg ml^{-1}; VLDL 12 μg ml^{-1}; Kin-1 8 μg ml^{-1}; Fibr 300 μg ml^{-1}. HP was depleted of HRG and KIN-1 by passing through a phosphocellulose matrix (see HRG purification) and by collecting the flow-through. After dialysis of 3 ml of plasma against 500 ml PBS at 4 °C for 18 h (PBS was changed after 3–4 h), the HRG/Kin-1 depleted plasma was quantitated for protein concentration and its activity was compared with normal HP similarly treated and dialyzed, normalizing for protein concentration differences. Dialyzed normal and HRG/Kin-1 depleted human plasma were supplemented with sodium citrate (0.38% v/v) to avoid coagulation and immediately used for cellular treatment or corona experiments.

FACS analysis

Monocytes and macrophages (2×10^6 cells per well; 1×10^6 cells per cm^2) seeded into 24-well plates (Falcon) were incubated at 37 °C for 3, 6 or 24 h with Stöber NPs (range: 0–80 μg ml^{-1}) under different conditions as indicated in figures. In other experiments, macrophages were pre-treated or not for 30′ at 37 °C with freshly prepared 10 mM sodium azide (Sigma Aldrich) plus 5 mM 2-deoxyglucose (Sigma Aldrich) in the presence of RPMI, RPMI+10% FCS, RPMI+10% HP or RPMI+15 μg ml^{-1} HRG. Then, Stöber NPs (20 μg ml^{-1}) were added for 2 h at 37 °C or 4 °C. HepG2 cells (1.5×10^5 cells per well) were seeded into 24-well plates the day before the experiment, and treated at 37 °C with Stöber NPs (0–50 μg ml^{-1}) for 20 h in RPMI, RPMI+10% FCS, and RPMI+10% HP. Cells were collected by plastic scraping (monocytes/macrophages) or trypsinisation (HepG2), washed with PBS, resuspended in cold FACS buffer (PBS, pH 7.4 + 1% FCS) supplemented with NH_4Cl 10 mM to neutralize acidic compartments to obtain the maximal FITC fluorescence, and stained with propidium iodide 15 μg ml^{-1} (Sigma Aldrich) to exclude dead cells. Samples were acquired with a BD FACSCanto II using FACSDiva software (Becton Dickinson) and NPs' association with live cells (10 000 events) was evaluated as mean fluorescence intensities (MFI). The contribution of traces of free

FITC in the NP preparation (<0.35% of particle coupled FITC) was estimated by testing the cells under the same conditions with equivalent quantities of NP ultra filtrates and found to account for <0.005% of the signal obtained using the corresponding FITC-labelled NP preparations.

SiO_2-NP protein corona determination

Stöber NPs were incubated under stirring at 37 °C or 4 °C for 15′, 3 h and 6 h in RPMI 1640 supplemented with 10% FCS, 10% or 100% HP or 10% MP (thawed at 37 °C and pre-centrifuged at 15 300*g* for 10′ at 4 °C to eliminate any aggregates), or the corona mix composed or depleted of each single protein (volume 1.5–2 ml). NPs were subsequently diluted with 9 ml of ice-cold PBS pH 7.4 in polycarbonate tubes (Beckman Coulter, cat. number 355603), immediately recovered by ultracentrifugation (45 minutes, 100 000*g* at 4 °C, XL-70 Ultracentrifuge Beckman, fixed angle 50 Ti rotor), washed twice with 10.5 ml of ice-cold PBS pH 7.4 and eventually dissolved in 75 μl of non-reducing loading sample buffer (62.5 mM Tris-HCl, pH 6.8, 2% SDS, 25% glycerol, 0.01% bromophenol blue). In separate experiments the NP yields after washing were estimated by comparing the absorbance of FITC in supernatants and the final pellets and found to be 95.5% ± 4 (mean ± SE; $N = 6$) of the total particles present before centrifugation. In other experiments, the SiO_2-NP protein corona was determined as described by Tenzer *et al.*[12] Briefly, 20 μg ml^{-1} Stöber NPs were incubated for 15′ at 37 °C or 4 °C in 10% or 100% pre-centrifuged HP in a volume of 2 ml, stratified onto a sucrose cushion (0.7 M in PBS, 2 ml) and centrifuged for 45′ at 100 000*g* at 4 °C using a swing out SW60 Ti rotor (Beckman Coulter) in 4 ml tubes (Beckman Coulter, cat. number 344062). After washing twice with 4 ml PBS and centrifuging as above, the NP pellet was dissolved in loading sample buffer. After heating at 95 °C for 5′ equal volumes (25 μl) or equal amounts (13.3 μg) of samples were subjected to gradient SDS-PAGE in 4–20% Mini-PROTEAN® TGXTM Precast Gel (Biorad). Mock samples were prepared using different protein mixtures or FCS/HP protein in the absence of NPs, to estimate the non-specific protein background. Proteins were stained with silver nitrate or with colloidal Coomassie G-250 in the case of mass spectrometry analysis, or transferred on a PVDF membrane for western blotting (see ESI† methods). Band intensities of NP associated proteins were estimated using ImageJ software after subtraction of any background signal (mock samples). The serially diluted known amounts of purified human plasma proteins were loaded in parallel in the same gel to obtain a calibration curve that allowed us to estimate the nmoles of each single protein associated with a given amount of NPs in nmoles corrected for the NP recovery after ultracentrifugation (a molecular weight of $\sim 10^7$ Da was assumed for SiO_2-NPs; three Apo A-I polypeptides were assumed to be present in one HDL lipoprotein). This allowed the quantification, after silver staining and densitometry, of the number of protein molecules per corona unit.

In-gel digestion, protein identification and database search

Excised from the gel, bands were washed with 50% v/v acetonitrile (ACN) in 0.1 M NH_4HCO_3, and vacuum-dried. For the faintest bands two bands from identical parallel lanes were extracted. The proteins were reduced for 30 min at 56 °C with 10 mM DTT in 0.1 M NH_4HCO_3. After cooling, the DTT solution was immediately replaced with 55 mM iodoacetamide in 0.1 M NH_4HCO_3 to alkylate the free SH groups for 20 min at 25 °C in the dark. After washing with 50% ACN in 0.1 M NH_4HCO_3, the dried gel pieces were swollen in 15 μl of digestion buffer containing 25 mM NH_4HCO_3 and 12.5 ng μl^{-1} trypsin (Promega, Madison, WI, USA) and incubated overnight at 37 °C. Tryptic peptides were extracted according to the protocol described by Kim *et al.*[26] Peptide mixtures were then analysed by LC MS/MS on a 6520 Q-TOF mass spectrometer (Agilent Technologies, Santa Clara, CA, USA) coupled to a chip-based chromatographic interface. Column volume loading varied from 1 to 4 microliters depending on the staining intensity of the corresponding treated bands, to ensure comparable analysis. A large capacity chip (C18, 150 μm × 75 μm) with an enrichment column (C18, 9 mm, 160 nl volume) was used to separate peptides at a flow rate of 0.3 μl min^{-1}. Water/formic acid 0.1% and acetonitrile/formic acid 0.1% were used as eluents A and B, respectively. Chromatographic separation was achieved with a gradient of B from 5% to 50% in 20 min. Raw data files were converted into the Mascot Generic Format (MGF) with MassHunter Qualitative Analysis Software version B.03.01 (Agilent Technologies) and analysed using Mascot Search Engine version 2.2.4 (Matrix Science). MS/MS spectra were searched against the SwissProt database, with the Mammalia taxonomy filter (June 2014 version, Taxonomy Mammalia, 66370 peptide entries). Enzyme specificity was set to trypsin/P with 2 missed cleavage, using a mass tolerance window of 20 ppm for parent mass and 0.6 Da for fragment ions. Carbamidomethylation of cysteine was set as fixed modification and methionine oxidation as variable modification. Proteins were considered positive hits if at least 2 peptides per protein were identified with high confidence ($p < 0.05$). The Exponentially Modified Protein Abundance Index (emPAI) was considered in order to calculate an approximate, label free, relative quantitation of the proteins.[32] The emPAI is calculated automatically by Mascot, emPAI = $10^{(N_{\text{observed}}/N_{\text{observable}})} - 1$ where $N_{\text{observable}}$ corresponds to the possible peptide hits generated by a given polypeptide based on *in silico* trypsinisation. Label free emPAI values were used, after correction for sample loading (number of bands, volume loaded for LC MS/MS) to calculate the molar% distribution of the main found proteins within the same SDS-PAGE lanes.

HRG purification

Human HRG was purified from human plasma as previously described[67,68] using a Fast Liquid chromatography (FPLC) system (Pharmacia). Briefly, 20 ml of a phosphocellulose resin (P11, Whatman) were equilibrated overnight at 4 °C with 10 volumes of loading buffer (10 mM sodium phosphate,

0.5 M NaCl, 1 mM EDTA, pH 6.8) supplemented with a protease inhibitor cocktail (Roche, cat. number 11873580001). Human plasma (50 ml) was centrifuged (12 000 rpm, 20′, 4 °C), diluted 1 : 1 with loading buffer 2×, passed through the equilibrated column, and the flow through was collected. After extensive washing (20 volumes) with 10 mM sodium phosphate, 0.8 M NaCl, 1 mM EDTA, pH 6.8, the bound HRG was eluted by a progressive saline gradient (from 0.8 M to 2 M NaCl) in the absence of protease inhibitors. HRG positive fractions (detected by silver staining and western blot analysis using anti-HRG mouse polyclonal antibody (Abnova, B01P) (see Fig. S12†) were dialyzed at 4 °C for 20 h against 20 volumes of PBS pH 7.4, quantified by the Bradford assay[69] using a Bio-Rad Protein Assay Dye reagent and stored in aliquots at −80 °C after freezing in liquid nitrogen. On average, 2.4–4.3 mg of protein were obtained from 50 ml human plasma. Thawed HRG aliquots were never re-frozen and re-used for experiments.

Determination of the K_d of protein–SiO_2-NP complexes

Increasing concentrations of purified human plasma proteins (HRG MW 64 kDa, Kin-1 MW 72 kDa, Fibr MW 340 kDa and HSA 60 kDa) were incubated with no particles or with SiO_2-NPs (100 μg ml^{-1}, ~10 nM, assuming a nanoparticle MW of ~10^7 Da) in PBS pH 7.4 at 37 °C for 15 min. After ultracentrifugation for 60 min at 100 000*g* using an Optima Max-E ultracentrifuge (Beckman), the concentration of free proteins in the supernatants (Pr^f) were measured by a Bradford colorimetric protein micro-assay. K_d and maximal binding capacity were obtained by plotting the bound particle *vs.* free protein concentration (nM) and best fitting non-linearly the data with the one-site equilibrium equation $Pr^b = Pr^f Pr^b_{max}/(Pr^f + K_d)$ (Origin mathematics package), where Pr^b is SiO_2-NP bound protein concentration, Pr^b_{max} is the maximal bound protein concentration and K_d is the dissociation constant.

Statistical analysis

Statistical analyses were performed using the Microcal Origin 8 software package. Gaussian distribution of data was checked by the Shapiro–Wilk test (0.05 level). Significance of the differences between means (0.05 level) was evaluated by using two samples or the paired *t* test, when applicable, by ANOVA analysis.

Acknowledgements

We thank the Centro Trasfusionale of the Hospital of Padua (ULSS 16) for providing buffy coats and human plasma, Dr Paolo di Muro for HRG purification assistance and Dr Giovanni Miotto (Proteomics Facility of the University of Padua) for technical assistance in mass-spectrometry analyses. This work was supported by the European Community's Seventh Framework Programme (FP7/2007–2013) under grant agreement no. 201031 NANOPHOTO, by the University of Padova (Ex 60%, 2010–2014, PRAT 2011, Progetto Strategico NAMECA) and by the Italian Ministry of Research (FIRB 2011, RBAP114AMK-RINAME).

Notes and references

1 P. Aggarwal, J. B. Hall, C. B. McLeland, M. A. Dobrovolskaia and S. E. McNeil, *Adv. Drug Delivery Rev.*, 2009, **61**, 428–437.
2 M. Lundqvist, J. Stigler, T. Cedervall, T. Berggard, M. B. Flanagan, I. Lynch, G. Elia and K. Dawson, *ACS Nano*, 2011, **5**, 7503–7509.
3 M. Lundqvist, J. Stigler, G. Elia, I. Lynch, T. Cedervall and K. A. Dawson, *Proc. Natl. Acad. Sci. U. S. A.*, 2008, **105**, 14265–14270.
4 N. P. Mortensen, G. B. Hurst, W. Wang, C. M. Foster, P. D. Nallathamby and S. T. Retterer, *Nanoscale*, 2013, **5**, 6372–6380.
5 C. D. Walkey, J. B. Olsen, F. Song, R. Liu, H. Guo, D. W. Olsen, Y. Cohen, A. Emili and W. C. Chan, *ACS Nano*, 2014, **8**, 2439–2455.
6 Z. J. Deng, M. Liang, I. Toth, M. Monteiro and R. F. Minchin, *Nanotoxicology*, 2013, **7**, 314–322.
7 A. Gessner, A. Lieske, B. R. Paulke and R. H. Muller, *J. Biomed. Mater. Res., Part A*, 2003, **65**, 319–326.
8 A. Gessner, R. Waicz, A. Lieske, B. Paulke, K. Mader and R. H. Muller, *Int. J. Pharm.*, 2000, **196**, 245–249.
9 T. Cedervall, I. Lynch, M. Foy, T. Berggard, S. C. Donnelly, G. Cagney, S. Linse and K. A. Dawson, *Angew. Chem., Int. Ed.*, 2007, **46**, 5754–5756.
10 R. R. Arvizo, K. Giri, D. Moyano, O. R. Miranda, B. Madden, D. J. McCormick, R. Bhattacharya, V. M. Rotello, J. P. Kocher and P. Mukherjee, *PLoS One*, 2012, **7**, e33650.
11 S. Tenzer, D. Docter, S. Rosfa, A. Wlodarski, J. Kuharev, A. Rekik, S. K. Knauer, C. Bantz, T. Nawroth, C. Bier, J. Sirirattanapan, W. Mann, L. Treuel, R. Zellner, M. Maskos, H. Schild and R. H. Stauber, *ACS Nano*, 2011, **5**, 7155–7167.
12 S. Tenzer, D. Docter, J. Kuharev, A. Musyanovych, V. Fetz, R. Hecht, F. Schlenk, D. Fischer, K. Kiouptsi, C. Reinhardt, K. Landfester, H. Schild, M. Maskos, S. K. Knauer and R. H. Stauber, *Nat. Nanotechnol.*, 2013, **8**, 772–781.
13 C. D. Walkey, J. B. Olsen, H. Guo, A. Emili and W. C. Chan, *J. Am. Chem. Soc.*, 2012, **134**, 2139–2147.
14 D. Walczyk, F. B. Bombelli, M. P. Monopoli, I. Lynch and K. A. Dawson, *J. Am. Chem. Soc.*, 2010, **132**, 5761–5768.
15 R. Huang, R. P. Carney, F. Stellacci and B. L. Lau, *Nanoscale*, 2013, **5**, 6928–6935.
16 U. Sakulkhu, L. Maurizi, M. Mahmoudi, M. Motazacker, M. Vries, A. Gramoun, M. G. Ollivier Beuzelin, J. P. Vallee, F. Rezaee and H. Hofmann, *Nanoscale*, 2014, **6**, 11439–11450.
17 S. Winzen, S. Schoettler, G. Baier, C. Rosenauer, V. Mailaender, K. Landfester and K. Mohr, *Nanoscale*, 2015, **7**, 2992–3001.

18 R. Liu, W. Jiang, C. D. Walkey, W. C. Chan and Y. Cohen, *Nanoscale*, 2015, **7**, 9664–9675.
19 M. A. Malvindi, V. Brunetti, G. Vecchio, A. Galeone, R. Cingolani and P. P. Pompa, *Nanoscale*, 2012, **4**, 486–495.
20 F. D. Sahneh, C. M. Scoglio, N. A. Monteiro-Riviere and J. E. Riviere, *Nanomedicine*, 2014, **9**, 1–9.
21 A. Lesniak, F. Fenaroli, M. P. Monopoli, C. Aberg, K. A. Dawson and A. Salvati, *ACS Nano*, 2012, **6**, 5845–5857.
22 N. A. Monteiro-Riviere, M. E. Samberg, S. J. Oldenburg and J. E. Riviere, *Toxicol. Lett.*, 2013, **220**, 286–293.
23 C. Fedeli, D. Segat, R. Tavano, G. De Franceschi, P. P. de Laureto, E. Lubian, F. Selvestrel, F. Mancin and E. Papini, *Nanomedicine*, 2014, **9**, 2481.
24 C. Fedeli, F. Selvestrel, R. Tavano, D. Segat, F. Mancin and E. Papini, *Nanomedicine*, 2012, **8**, 1101.
25 Y. Yan, K. T. Gause, M. M. Kamphuis, C. S. Ang, N. M. O'Brien-Simpson, J. C. Lenzo, E. C. Reynolds, E. C. Nice and F. Caruso, *ACS Nano*, 2013, **7**, 10960–10970.
26 J. A. Kim, A. Salvati, C. Aberg and K. A. Dawson, *Nanoscale*, 2014, **6**, 14180–14184.
27 E. Izak-Nau, M. Voetz, S. Eiden, A. Duschl and V. F. Puntes, *Part. Fibre Toxicol.*, 2013, **10**, 56.
28 T. M. Forte, J. J. Bell-Quint and F. Cheng, *Lipids*, 1981, **16**, 240–245.
29 W. Stöber, A. Fink and E. Bohn, *J. Colloid Interface Sci.*, 1968, **26**, 62–69.
30 A. Van Blaaderen and A. Vrij, *J. Colloid Interface Sci.*, 1993, **156**, 1–18.
31 A. Van Blaaderen and A. Vrij, *Langmuir*, 1992, **8**, 2921–2931.
32 Y. Ishihama, Y. Oda, T. Tabata, T. Sato, T. Nagasu, J. Rappsilber and M. Mann, *Mol. Cell. Proteomics*, 2005, **4**, 1265–1272.
33 A. K. Rai, B. Spolaore, D. A. Harris, F. Dabbeni-Sala and G. Lippe, *J. Bioenerg. Biomembr.*, 2013, **45**, 569–579.
34 M. P. Monopoli, D. Walczyk, A. Campbell, G. Elia, I. Lynch, F. B. Bombelli and K. A. Dawson, *J. Am. Chem. Soc.*, 2011, **133**, 2525–2534.
35 C. Rocker, M. Potzl, F. Zhang, W. J. Parak and G. U. Nienhaus, *Nat. Nanotechnol.*, 2009, **4**, 577–580.
36 P. Maffre, S. Brandholt, K. Nienhaus, L. Shang, W. J. Parak and G. U. Nienhaus, *Beilstein J. Nanotechnol.*, 2014, **5**, 2036–2047, DOI: 10.3762/bjnano.5.212.
37 B. Pelaz, P. Del Pino, P. Maffre, R. Hartmann, M. Gallego, S. Rivera-Fernandez, J. M. de la Fuente, G. U. Nienhaus and W. J. Parak, *ACS Nano*, 2015, **9**, 6996–7008, DOI: 10.1021/acsnano.5b01326.
38 A. S. Shah, L. Tan, J. L. Long and W. S. Davidson, *J. Lipid Res.*, 2013, **54**, 2575–2585.
39 T. Vaisar, S. Pennathur, P. S. Green, S. A. Gharib, A. N. Hoofnagle, M. C. Cheung, J. Byun, S. Vuletic, S. Kassim, P. Singh, H. Chea, R. H. Knopp, J. Brunzell, R. Geary, A. Chait, X. Q. Zhao, K. Elkon, S. Marcovina, P. Ridker, J. F. Oram and J. W. Heinecke, *J. Clin. Invest.*, 2007, **117**, 746–756.
40 M. Dashty, M. M. Motazacker, J. Levels, M. de Vries, M. Mahmoudi, M. P. Peppelenbosch and F. Rezaee, *Thromb. Haemostasis*, 2014, **111**, 518–530.
41 S. Laurent, C. Burtea, C. Thirifays, F. Rezaee and M. Mahmoudi, *J. Colloid Interface Sci.*, 2013, **392**, 431–445.
42 S. Wan, P. M. Kelly, E. Mahon, H. Stockmann, P. M. Rudd, F. Caruso, K. A. Dawson, Y. Yan and M. P. Monopoli, *ACS Nano*, 2015, **9**, 2157–2166.
43 W. Liu, J. Rose, S. Plantevin, M. Auffan, J. Y. Bottero and C. Vidaud, *Nanoscale*, 2013, **5**, 1658–1668.
44 D. Dell'Orco, M. Lundqvist, C. Oslakovic, T. Cedervall and S. Linse, *PLoS One*, 2010, **5**, e10949.
45 M. P. Monopoli, D. Walczyk, A. Campbell, G. Elia, I. Lynch, F. B. Bombelli and K. A. Dawson, *J. Am. Chem. Soc.*, 2011, **133**, 2525–2534.
46 K. Sempf, T. Arrey, S. Gelperina, T. Schorge, B. Meyer, M. Karas and J. Kreuter, *Eur. J. Pharm. Biopharm.*, 2013, **85**, 53–60.
47 P. P. Karmali, Y. Chao, J. H. Park, M. J. Sailor, E. Ruoslahti, S. C. Esener and D. Simberg, *Mol. Pharm.*, 2012, **9**, 539–545.
48 O. Kassaar, S. A. McMahon, R. Thompson, C. H. Botting, J. H. Naismith and A. J. Stewart, *Blood*, 2014, **123**, 1948–1955.
49 P. S. Nair and W. E. Robinson, *Arch. Biochem. Biophys.*, 1999, **366**, 8–14.
50 I. K. Poon, K. K. Patel, D. S. Davis, C. R. Parish and M. D. Hulett, *Blood*, 2011, **117**, 2093–2101.
51 D. B. Borza and W. T. Morgan, *J. Biol. Chem.*, 1998, **273**, 5493–5499.
52 A. L. Jones, M. D. Hulett and C. R. Parish, *Immunol. Cell Biol.*, 2005, **83**, 106–118.
53 V. Rydengard, A. K. Olsson, M. Morgelin and A. Schmidtchen, *FEBS J.*, 2007, **274**, 377–389.
54 V. Rydengard, O. Shannon, K. Lundqvist, L. Kacprzyk, A. Chalupka, A. K. Olsson, M. Morgelin, W. Jahnen-Dechent, M. Malmsten and A. Schmidtchen, *PLoS Pathog.*, 2008, **4**, e1000116.
55 O. Shannon, V. Rydengard, A. Schmidtchen, M. Morgelin, P. Alm, O. E. Sorensen and L. Bjorck, *Blood*, 2010, **116**, 2365–2372.
56 J. W. Bryant and Z. Shariat-Madar, *Cardiovasc. Hematol. Agents Med. Chem.*, 2009, **7**, 234–250.
57 R. Tavano, D. Segat, E. Reddi, J. Kos, M. Rojnik, P. Kocbek, S. Iratni, D. Scheglmann, M. Colucci, I. M. Echevarria, F. Selvestrel, F. Mancin and E. Papini, *Nanomedicine*, 2010, **5**, 881–896.
58 N. Sheng, M. B. Fairbanks, R. L. Heinrikson, G. Canziani, I. M. Chaiken, D. M. Mosser, H. Zhang and R. W. Colman, *Blood*, 2000, **95**, 3788–3795.
59 S. K. Lee and J. L. Ding, *DNA Cell Biol.*, 2013, **32**, 36–40.
60 K. Poon, M. D. Hulett and C. R. Parish, *Blood*, 2010, **115**, 2473–2482.
61 K. K. Patel, I. K. Poon, G. H. Talbo, M. A. Perugini, N. L. Taylor, T. J. Ralph, N. J. Hoogenraad and M. D. Hulett, *IUBMB Life*, 2013, **65**, 550–563.

62 L. L. Leung, *J. Clin. Invest.*, 1986, **77**, 1305–1311.
63 C. Rolny, M. Mazzone, S. Tugues, D. Laoui, I. Johansson, C. Coulon, M. L. Squadrito, I. Segura, X. Li, E. Knevels, S. Costa, S. Vinckier, T. Dresselaer, P. Akerud, M. De Mol, H. Salomaki, M. Phillipson, S. Wyns, E. Larsson, I. Buysschaert, J. Botling, U. Himmelreich, J. A. Van Ginderachter, M. De Palma, M. Dewerchin, L. Claesson-Welsh and P. Carmeliet, *Cancer Cell*, 2011, **19**, 31–44.
64 S. Tugues, S. Honjo, C. Konig, O. Noguer, M. Hedlund, J. Botling, S. Deschoemaeker, M. Wenes, C. Rolny, W. Jahnen-Dechent, M. Mazzone and L. Claesson-Welsh, *Cancer Res.*, 2012, **72**, 1953–1963.
65 R. Tavano, S. Franzoso, P. Cecchini, E. Cartocci, F. Oriente, B. Arico and E. Papini, *J. Leukocyte Biol.*, 2009, **86**, 143–153.
66 J. L. Callum, K. Karkouti and Y. Lin, *Transfus. Med. Rev.*, 2009, **23**, 177–188.
67 A. L. Jones, I. K. Poon, M. D. Hulett and C. R. Parish, *J. Biol. Chem.*, 2005, **280**, 35733–35741.
68 D. B. Rylatt, D. Y. Sia, J. P. Mundy and C. R. Parish, *Eur. J. Biochem.*, 1981, **119**, 641–646.
69 M. M. Bradford, *Anal. Biochem.*, 1976, **72**, 248–254.